QC
879.5
U45
no. 51

Suppl.
no. 2

U.S. DEPARTMENT OF COMMERCE
Frederick B. Dent, Secretary

NATIONAL OCEANIC AND ATMOSPHERIC ADMINISTRATION
Robert M. White, Administrator

NATIONAL ENVIRONMENTAL SATELLITE SERVICE
David S. Johnson, Director

Supplement # 2 to
ESSA TECHNICAL REPORT NESC 51
(Also issued as Air Weather Service Technical Report No. 212)

Application of Meteorological Satellite Data in Analysis and Forecasting

Skidmore, Rance W., USAF
Purdom, James F. W., NOAA

WASHINGTON, D.C.
MARCH 1973

For sale by the Superintendent of Documents, U.S. Government Printing Office
Washington, D.C. 20402 - Price: 85 cents, domestic postpaid; 60 cents, GPO Bookstore
Stock Number 0314-00314

National Oceanic and Atmospheric Administration
TIROS Satellites and Satellite Meteorology

ERRATA NOTICE

One or more conditions of the original document may affect the quality of the image, such as:

Discolored pages
Faded or light ink
Binding intrudes into the text

This has been a co-operative project between the NOAA Central Library and the Climate Database Modernization Program, National Climate Data Center (NCDC). To view the original document contact the NOAA Central Library in Silver Spring, MD at (301) 713-2607 x124 or Library.Reference@noaa.gov.

HOV Services
Imaging Contractor
12200 Kiln Court
Beltsville, MD 20704-1387
January 26, 2009

NOAA

U.S. NATIONAL OCEANIC AND ATMOSPHERIC ADMINISTRATION

DEPARTMENT OF COMMERCE

PREFACE

This supplement to ESSA Technical Report NESC 51, "Application of Meteorological Satellite Data in Analysis and Forecasting", (also issued as Air Weather Service Technical Report No. 212) adds the following: Chapter 2, Glossary, section on Mountain Waves; Chapter 3, Synoptic Cloud Patterns, sections on Back-Door Cold Front, Cyclonically-Curved Cirrus Bands, and Mean Wind Speed in the Troposphere; Chapter 5, Local Phenomena, sections on Fog and Stratus, Turbulence, Mesoscale and Subsynoptic-Scale Vortices, Severe Weather and Sea Breeze.

These sections were compiled by the combined efforts of the following personnel:

National Environmental Satellite Service, National Oceanic and Atmospheric Administration:

James F. W. Purdom, Primary Author
Vincent J. Oliver, Contributor
Ralph K. Anderson, Contributor
Edward W. Ferguson, Contributor
LaRue F. Amacher, Illustrator

USAF Environmental Technical Applications Center (Air Weather Service):

Rance W. Skidmore, Capt, USAF, Primary Author
Jerome O. Siebers, Maj, USAF, Contributor
Arthur H. Smith, Contributor*
Elden C. Taylor, Capt, USAF, Contributor
Wayne Neff, Sgt, USAF, Illustrator

This supplement should be filed as part of ESSA TR NESC 51 (AWS TR 212). Pages v-viii of this supplement replace original pages v-vii. File pages R-5 and R-6 after R-4. File the sections of Chapters 2, 3 and 5 in the appropriate numbered sequence. File the cover sheet of this supplement immediately after cover sheet of first supplement and file this page immediately after page iii of the first supplement.

*Now with Field Services Division, National Environmental Satellite Service.

Blank page retained for pagination

TABLE OF CONTENTS

	Page
Chapter 1 - INTRODUCTION	1
Chapter 2 - SATELLITE CLOUD ATLAS AND GLOSSARY	2-1
Chapter 3 - SYNOPTIC CLOUD PATTERNS	
Vorticity and Vortices	3-A-1
Introduction	1
Vorticity	2
Enhanced Cumulus	2
Comma-Shaped Cloud Patterns	2
Vortex Development in the Cold Air	2
Vortex Development Along a Frontal Band	4
Wave Stage	4
Occluding Stage	6
Mature Stage	7
Dissipating Stage	8
Cut-Off Lows	10
Fronts	3-B-1
Introduction	1
Cold Fronts	2
Warm Fronts	6
Occluded Fronts	7
"Occluded" Frontogenesis	8
Fronts Over Land and Water	11
Non-Frontal Cloud Bands	12
Squall Lines	14
Back-Door Cold Front	15
Cellular Clouds	3-C-1
Introduction	1
Cellular Cloud Patterns	2
Open Cellular Cloud Patterns	6
Closed Cellular Cloud Patterns	8
Transitional Features	10
Cellular Clouds Over Land	11
Jet Streams	3-D-1
Introduction	1
Cirrus Shields and Shadow Lines	2
Cirrus Streaks	6
Transverse Lines	7
Cellular Cloud Patterns	8
Non-Jet Stream Cloud Patterns	10
Cyclonically-Curved Cirrus Bands	11
Upper Level Troughs	3-E-1
Introduction	1
Locating Troughs from Frontal Bands	2
Locating Troughs from Vorticity Maxima	4
Locating Troughs from Cirrus Clouds	5
Locating Troughs from Major Cloud Masses	6

Upper Level Ridges 3-F-1
Introduction. 1
Sharp Ridges. 2
Medium Ridges 4
Broad Ridges. 6
Minor Ridges. 8
Omega Blocks 8
Large-Scale Flow 9
Thermal Patterns 3-G-1
Introduction. 1
Surface Waves 3
Thickness Ridges and Mature Cyclones. 5
Dissipating Vortex and Thermal Trough 6
Thickness Troughs 7
Positive Vorticity Advection Maxima and Vorticity Centers . . . 8
Cut-Off Cyclones. 10
Surface Ridges 3-H-1
Introduction. 1
Northern Hemisphere 2
Type A 2
Type B 4
Type C 6
Type C (Variation) 8
Southern Hemisphere 9
Sun Glint 15
Surface Wind Direction and Speed 3-I-1
Introduction. 1
Cumulus Patterns to the Rear of Polar Fronts. 2
Wind Direction 2
Wind Speed 4
Wind Speed from Narrow Cloud Lines Near Continents. 5
Wind Direction from Sea Breeze. 6
Wind Speed from Sun Glint 8
Wind Direction from Island Effects. 9
Wind Information from Anomalous Cloud Lines 10
Wind Direction from Ice Movement. 11
Wind Direction from Orographic Effects. 12
Mean Wind Speed in the Troposphere 3-J-1

Chapter 4 - APPLICATION OF SATELLITE DATA TO SYNOPTIC ANALYSIS IN THE TROPICS
Introduction 4-A-1
Seasonal Changes in Tropical Cloud Distribution. 4-B-1
Subtropical Jet Streams. 4-C-1
Estimating Winds from Satellite Data 4-D-1
Introduction. 1
Estimating Upper Winds from Cumulonimbus Plumes 1
Estimating Upper Level Flow from Cirrus Cloud Shields 3
Rules and Guidelines for Estimating High-Level Wind Speed . . . 4
Estimating Low-Level Winds from Cumulus Cloud Lines 5
Wind Estimates from Geostationary Satellite Data. 6
Tropical Storms. 4-E-1
Introduction. 1

Current Classification System 1
Stage A. 3
Stage B. 4
Stage C. 5
Stage X. 6
Category 1 7
Category 2 7
Category 3 8
Category 4 9
Estimating the Winds in Stage X Storms. 9
Classifying Storms from Infrared Data 11
Weak Tropical Disturbances 4-F-1
Introduction. 1
Easterly Waves in the Tropical Atlantic - The "Inverted V" Formation 5
Disturbances Associated with the Mid-Pacific and Mid-Atlantic Troughs 8
Equatorial Anticyclones and "Burst Band" Disturbances 16
Frontal Shear Lines. 4-G-1
Interaction Between High and Low Latitudes in the Northern Hemisphere 4-H-1
Diurnal Cloud Changes in the Tropics 4-I-1

Chapter 5 - LOCAL PHENOMENA
Snow Cover and Snow Depth. 5-A-1
Introduction. 1
Snow Identification 2
Interpretation of Snow Depth. 6
Procedure for Snow-Depth Mapping in Non-Forested Areas. 8
Fog and Stratus. 5-B-1
Introduction. 1
Radiation Fog 2
Other Fog Types 4
Turbulence 5-C-1
Introduction. 1
Mountain Waves. 2
Jet Streams 3
Convection. 4
Other Turbulent Regions 6
Mesoscale and Subsynoptic-Scale Vortices 5-D-1
Introduction. 1
Mesoscale Vortices in Stratocumulus 2
Mesoscale Vortices in Cumulus Clouds. 3
Mesoscale Vortices in Fog 5
Subsynoptic-Scale Vortices. 6
Severe Weather 5-E-1
Introduction. 1
Squall Lines. 2
Locating the 850-mb Wind Maximum. 2
Middle and Upper Level Jets 2
Detection of Shear. 6
Squall Line Growth Characteristics as Observed by ATS-3 6
Isolation of Threat Areas 7

The Tornado Outbreak of May 5, 1971-An Illustrative Example . . 8
Sea Breeze 5-F-1
Introduction. 1
Sea Breeze Cloud Patterns 3

Chapter 6 - INFRARED
Basic Characteristics of Infrared Data 6-A-1
Introduction. 1
IR and Television Pictures Compared 1
Effects of Naturally-Occurring Temperature Variations on IR Pictures. 4
Identifying Synoptic-Scale Cloud Systems in IR. 6
Interpretation of Cloud Forms and Surface Features 6-B-1
Cirrus and Middle Cloud 1
Cumulus 14
Fog and Stratus 22
Earth's Surface 26
Appendix 6-C-1
Infrared Radiation from the Earth and Atmosphere. 1
Effects of Atmospheric Absorption (Limb-Darkening). 2
The Scanning Radiometer 3
Spatial Resolution of the SR. 4
Effect of Spatial Resolution on Indicated Cloud-Top Temperatures. 5
Temperature Resolution of the SR. 7
Conversion of Measured Radiances to Temperature 7
Computer-Processed IR Data. 7
Mapped NOAA Data. 8
Enhanced Displays 10
Enhancement of IR Imagery to Compensate for Latitude Temperature Changes 10
Enhancement of IR Imagery to Optimize the Display of Clouds in Certain Temperature Ranges 13

REFERENCES R1

WAVE CLOUDS - Wave clouds caused by terrain barriers appear as a pattern of vermiculated bands that range from a few miles up to 20 miles in width. The bands are separated by clear spaces of the same size. The appearance of wave clouds may vary depending on the shape of the barrier. These patterns usually consist of stratocumulus and altocumulus.

These criteria must be met for formation of mountain wave clouds: (1) Wind direction is more or less perpendicular to the mountains through a deep layer of the atmosphere, (2) winds at the top of the mountain are at least 25 knots, (3) winds increase steadily with height to about 300-mb., (4) the atmosphere is stable for vertical displacement of air parcels and, (5) sufficient moisture for cloud formation is present.

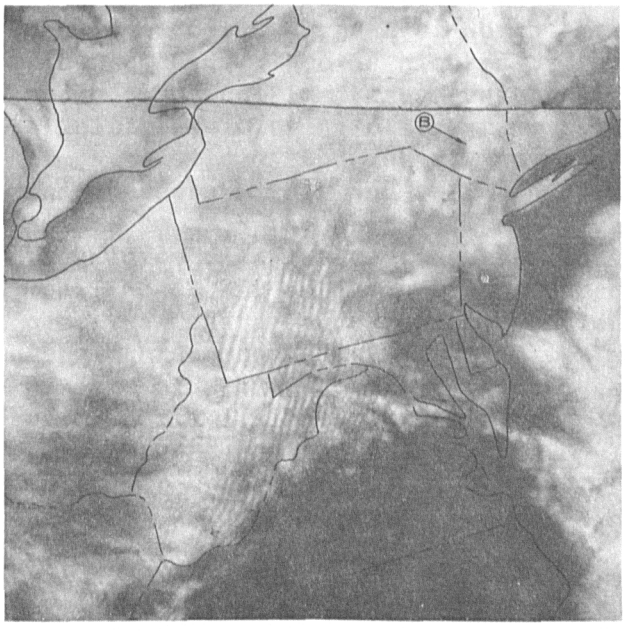

E-8 752- 1455 GMT February 13, 1967

Figure 2-54. Wave clouds associated with the Appalachian Mountains extend southward from central Pennsylvania into North Carolina. This pattern lies under the jet stream. A second area with waves of shorter length (B) lies just east of the Catskill Mountains. The cloud type forming the waves is predominately stratocumulus.

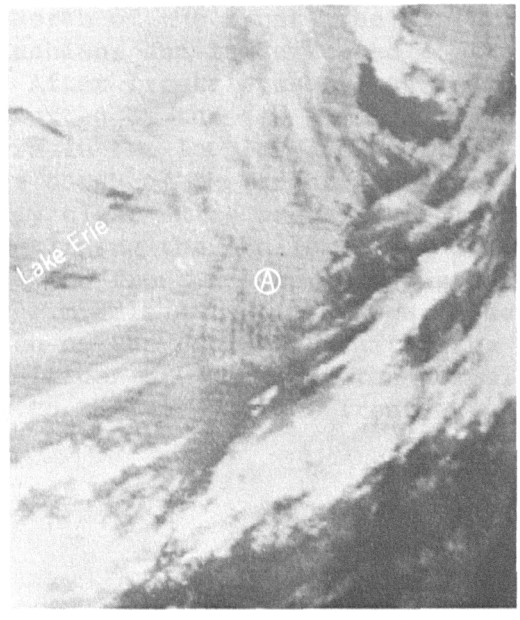

IR ITOS-1 0800 GMT December 20, 1970

Figure 2-55. Wave clouds (A) produced by the Appalachian Mountains are over eastern Pennsylvania. These wave clouds are at a relatively low level and show a small thermal contrast with the surrounding earth's surface. The cloud-free portion of Lake Huron appears dark in the upper left-hand corner of the picture; the warmer waters of the Atlantic appear dark on the eastern side of the picture.

Back-Door Cold Front

One of the many ways in which the Middle Atlantic States get temporary relief from hot, humid weather conditions is by the passage of a back-door cold front. Fronts of this type move towards the south or southeast along the Atlantic seaboard of the United States (57) and displace a westerly or southwesterly flow of warm, humid maritime tropical (mT) air with a cool northeast flow of modified continental polar (cP) air.

The 500-mb flow associated with a back-door cold front has a northerly component over eastern Canada. This northerly component occurs when a 500-mb ridge intensifies as it moves from central to eastern Canada. Concurrently a 500-mb low deepens and moves south over eastern Canada. As the 500-mb flow increases in amplitude, the surface high in eastern Canada strengthens and moves off the coast of North America. North of the front, the easterly flow at the surface is blocked by the Appalachians and is deflected to the south, undercutting the prevailing mT air. After frontal passage there is a significant lowering of the temperature and often of the dew point. Many times low clouds and fog are advected onshore in the low level easterly flow which occurs within one to two hundred miles north of the front. Further north, towards the center of the high, mostly clear skies prevail. This cloudiness aids in locating the front and outlining the shallow layer of cool modified cP air as it moves southward behind the front and spreads westward over the Coastal and Piedmont sections of the Middle Atlantic States. The Appalachian Mountains limit the westward push of the cool air. After the passage of a back-door cold front, cool conditions prevail over the normally warm, humid lowlands while in the mountains to the west of the front, high temperatures continue.

A back-door cold front moving southward along the Atlantic Coast is seen on the ESSA-9 photographs (Figures 3-B-17 and 3-B-18) at approximately 1800 GMT on May 14 and 15, 1970. The 24-hour movement of the frontal system can be traced with the satellite cloud patterns. Along the coastal area, the front moves southward from Delaware to South Carolina, while from the mountains west, the front moves northward from western Maryland to Canada. On both days most of the cloudiness is north of the front. The southern and western edges of the clouds outline the southern and western limits of the cool air. On the 15th, the clouds behind the front cover the Coastal and Piedmont sections of the Middle Atlantic States where an onshore flow takes place in the shallow layer of cool air.

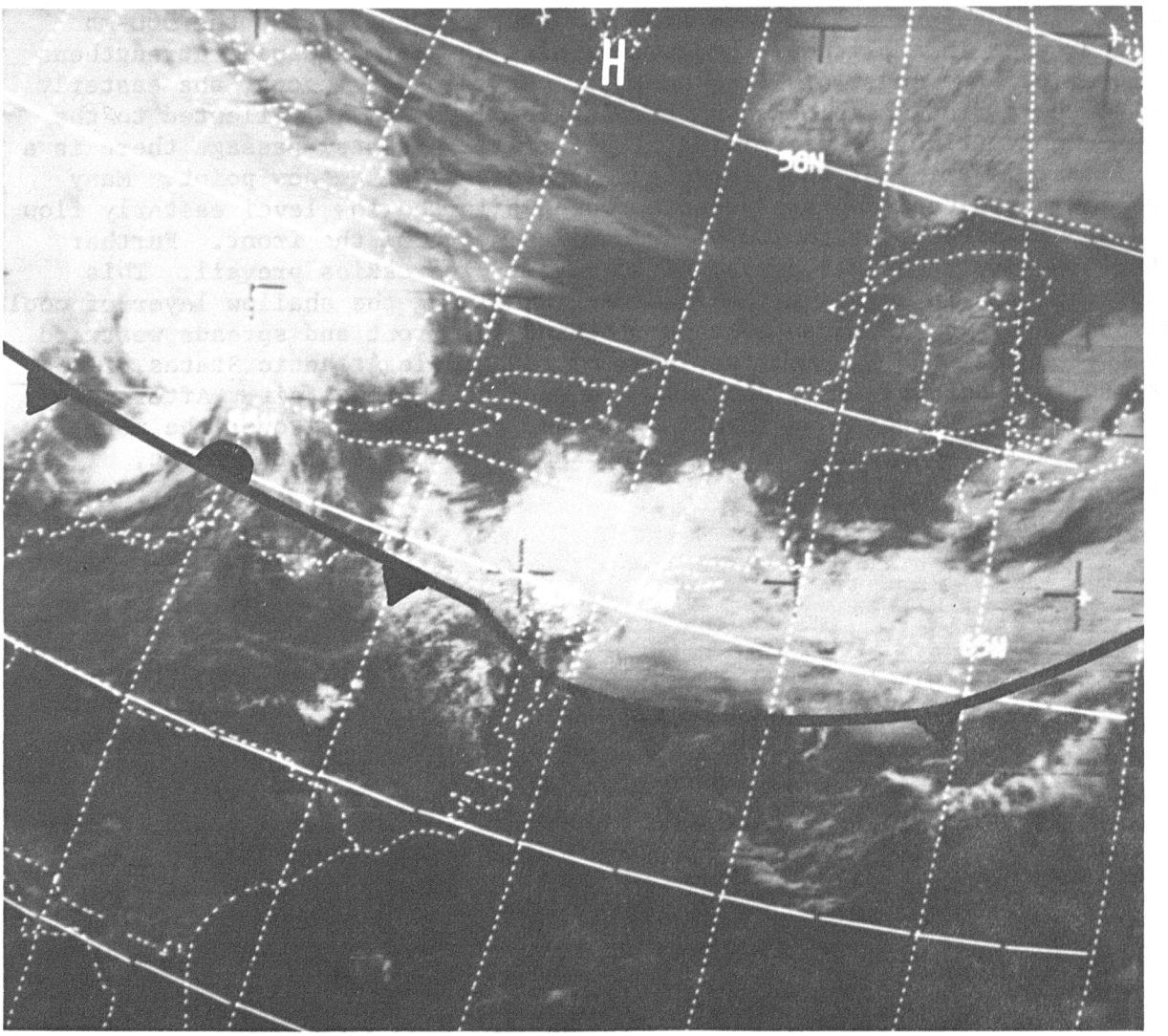

E-9 5526-4 1857 GMT May 14, 1970;Surface Front 1800 GMT May 14, 1970.

Figure 3-B-17. Clouds associated with onshore easterly winds behind a back-door cold front. Maximum temperatures (Fahrenheit) are in the 90's south of the front and between 70 and 80 in the cloudy zone north of the front. The center of the surface high is indicated by H.

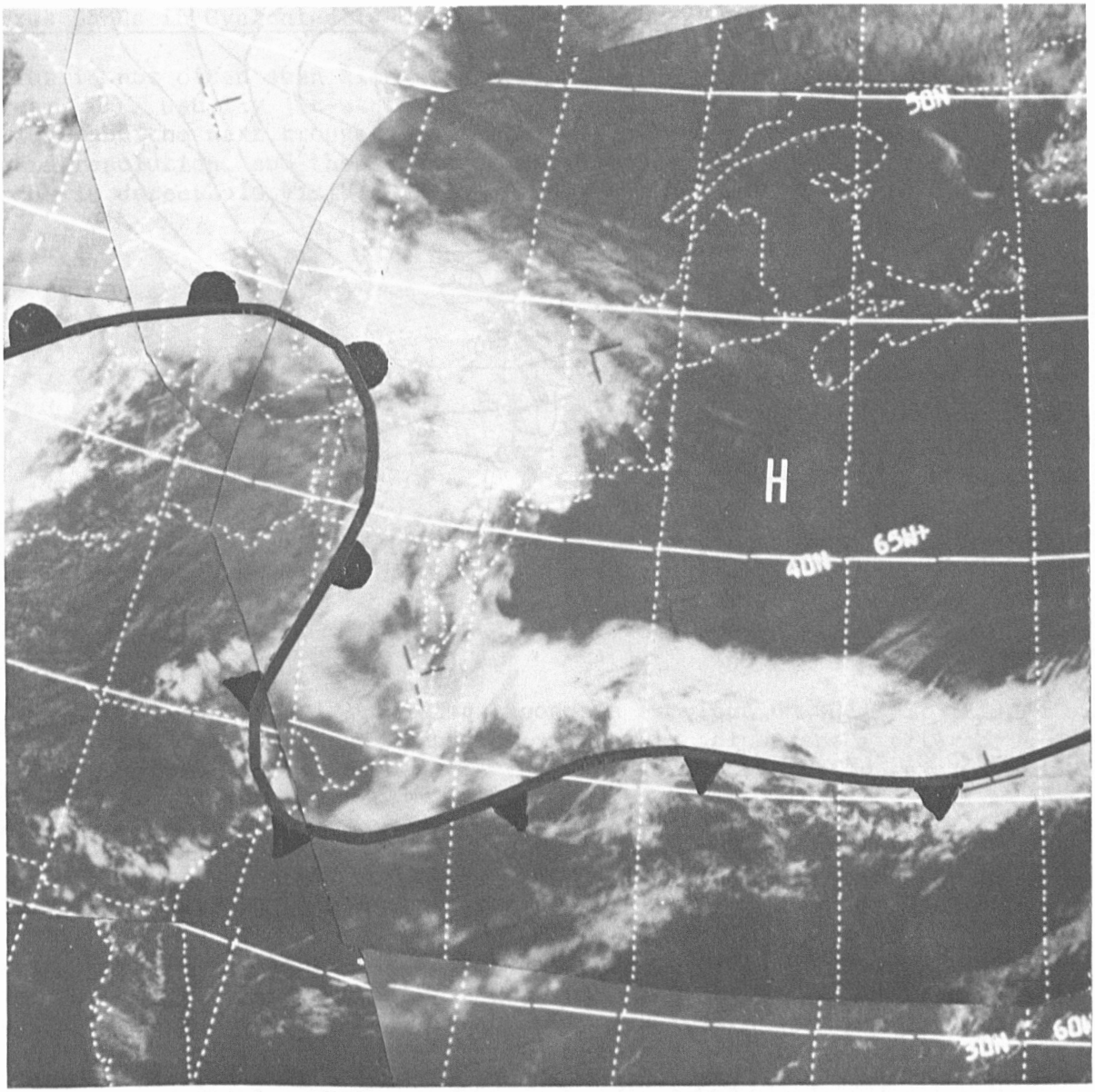

E-9 Mosaic of Pass 5538 (1800 GMT) and Pass 5539 (1955 GMT) May 15, 1970; Surface Front for 1800 GMT May 15, 1970.

Figure 3-B-18. Fog and stratus over the Piedmont and coastal sections of the Middle Atlantic States outline the southwestward extent of the shallow layer of modified cP air. The surface front continues to lie along the leading edge of the cloud band. Maritime tropical air to the south and west is characterized by some cumulonimbus and much fair weather cumulus. Maximum temperatures are near 70°F in the cloudy cold air north of the front and in the 90's south of the front. The Washington sounding showed marked cooling below 850 mb. The center of the surface high is indicated by H.

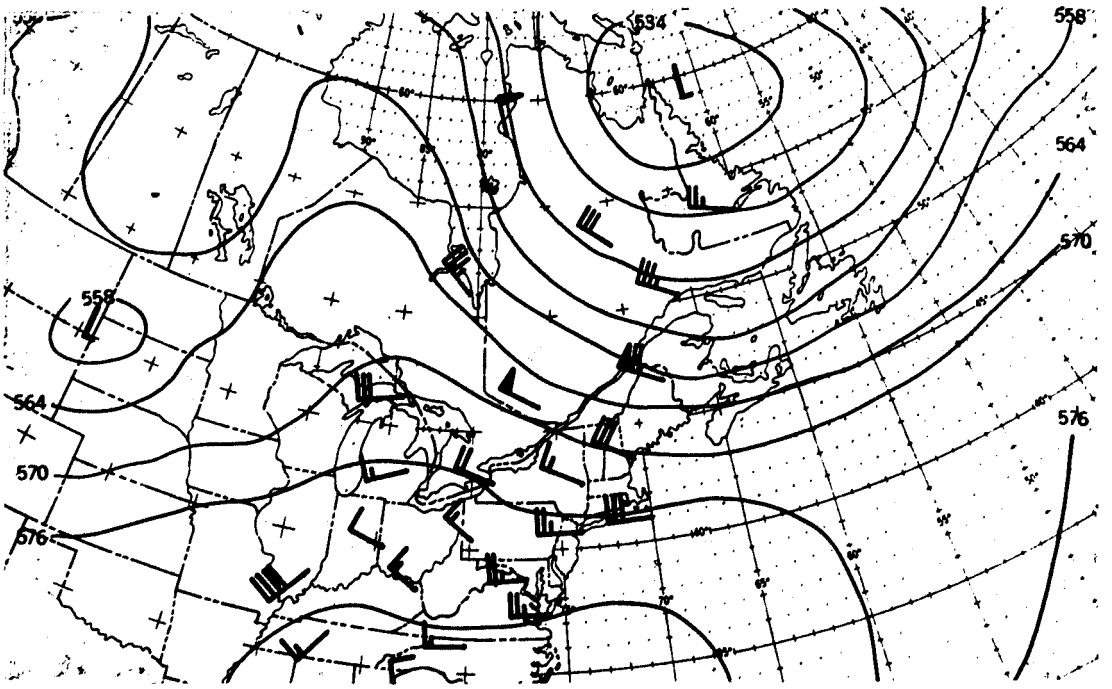

500-mb Analysis 1200 GMT May 14, 1970.

Figure 3-B-19. The 500-mb analysis six hours prior to figure 3-B-17. At this time there is a sharpening ridge over central Canada with closed lows over South Dakota and northern Labrador.

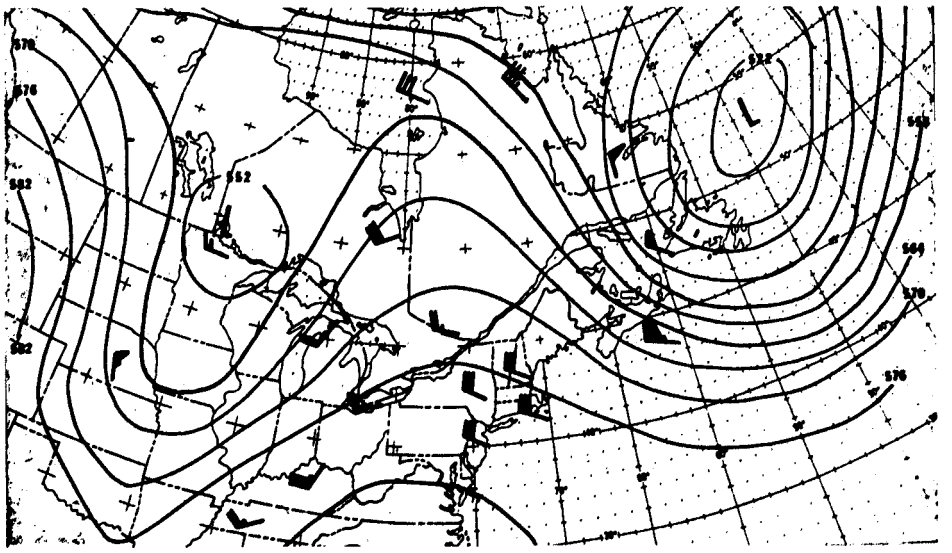

500-mb Analysis 0000 GMT May 16, 1970.

Figure 3-B-20. The 500-mb analysis six hours after figure 6-B-18. The axis of the ridge is over eastern Canada and the Labrador low has moved southeastward.

Cirrus Bands in Cyclonically-Curved Flow

Cirrus is not often seen along the cyclonically-curved portion of the jet stream (58). Usually jet-stream cirrus dissipates in the sinking air between a ridge and the next trough downstream. If cirrus is present, sun angle, camera resolution, and the amount of cirrus determine whether or not the cirrus is detectable visible data.

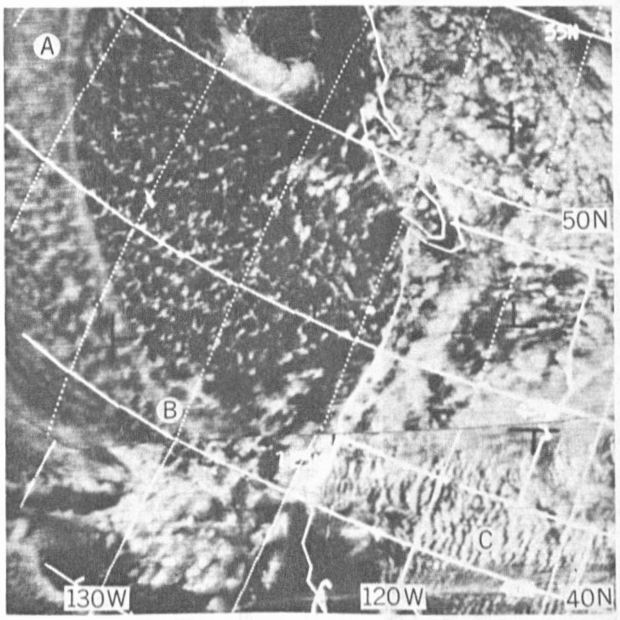

E-9 5290-3, 4 2130 GMT 25 April 1970

Figure 3-D-10. An extensive sheet of thin cirrus, associated with the cyclonically-curved portion of the polar jet stream, extends from A to B. The large area of mountain wave clouds at C is further evidence of this belt of strong winds. The difference in cellular cloud type across the jet axis west of B is less than usual. The normal pattern of open cells poleward of the jet and closed cells equatorward appears between B and the coast.

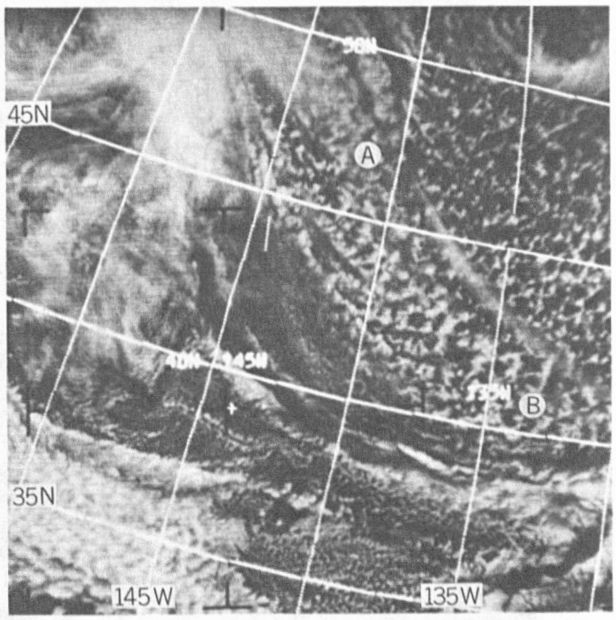

E-9 5291-4 2330 GMT 25 April 1970

Figure 3-D-11. Cirrus associated with the jet stream extends from A to B. This photograph is approximately two hours later than Figure 3-D-10 and illustrates the rapid dissipation of the cirrus during the 2-hour period.

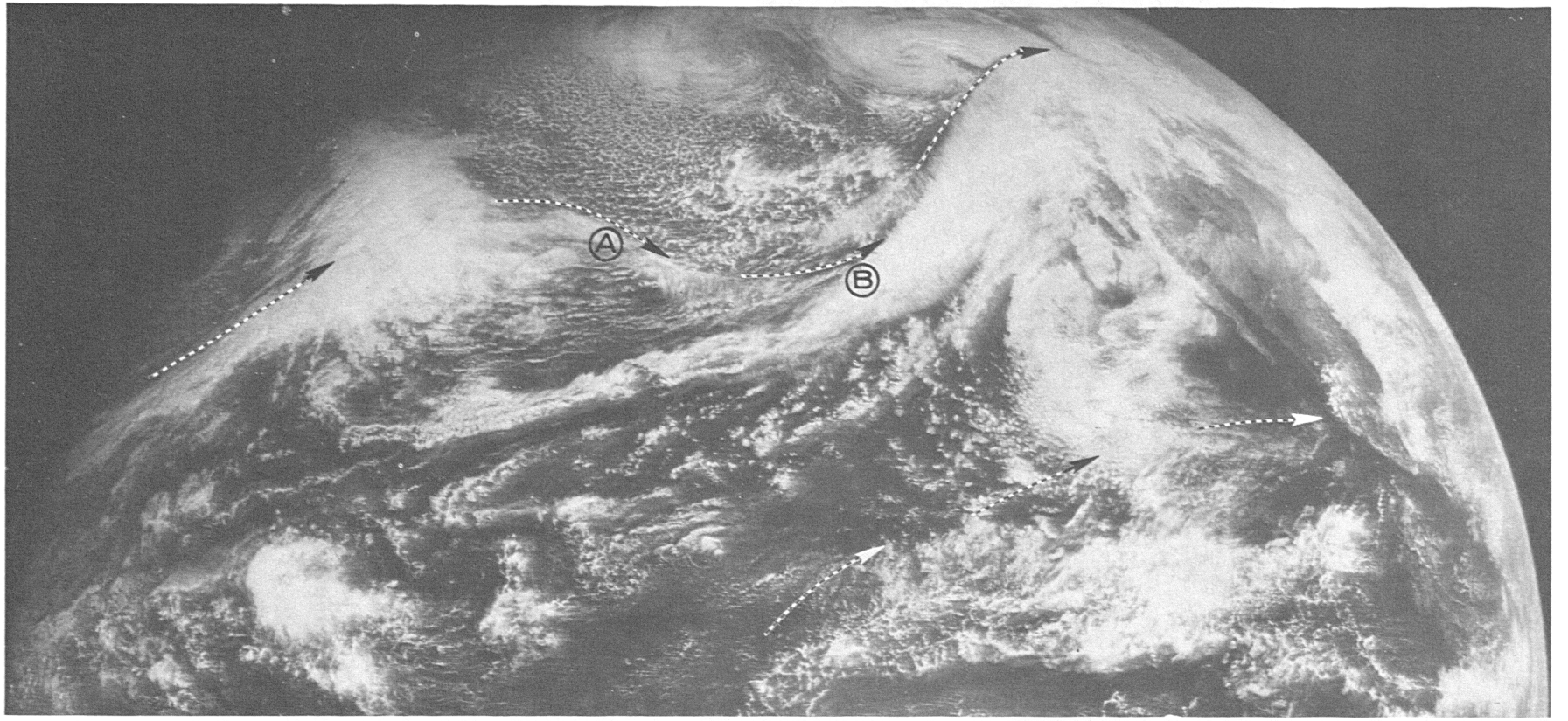

ATS-1 2043 GMT January 22, 1970. 200-mb Jet Superimposed.

Figure 3-D-12. Cyclonically curved cirrus associated with the polar jet stream is seen between A and B. It is unusual to observe as much cirrus through the trough as is visible here. An ill-defined subtropical jet stream to the south is weak so the cirrus associated with it has no sharply defined northern edge.

Chapter 3

SECTION J

MEAN WIND SPEED IN THE TROPOSPHERE

An estimate of the mean wind speed through the troposphere (U) can be obtained from wave clouds by using the equation U = 6L + 10 where L = the wavelength, in nautical miles, which is obtained by measuring the total distance covered by a representative sample of mountain wave clouds divided by the number of wave clouds in the sample (59). The equation shows that wind speed increases as wavelength increases.

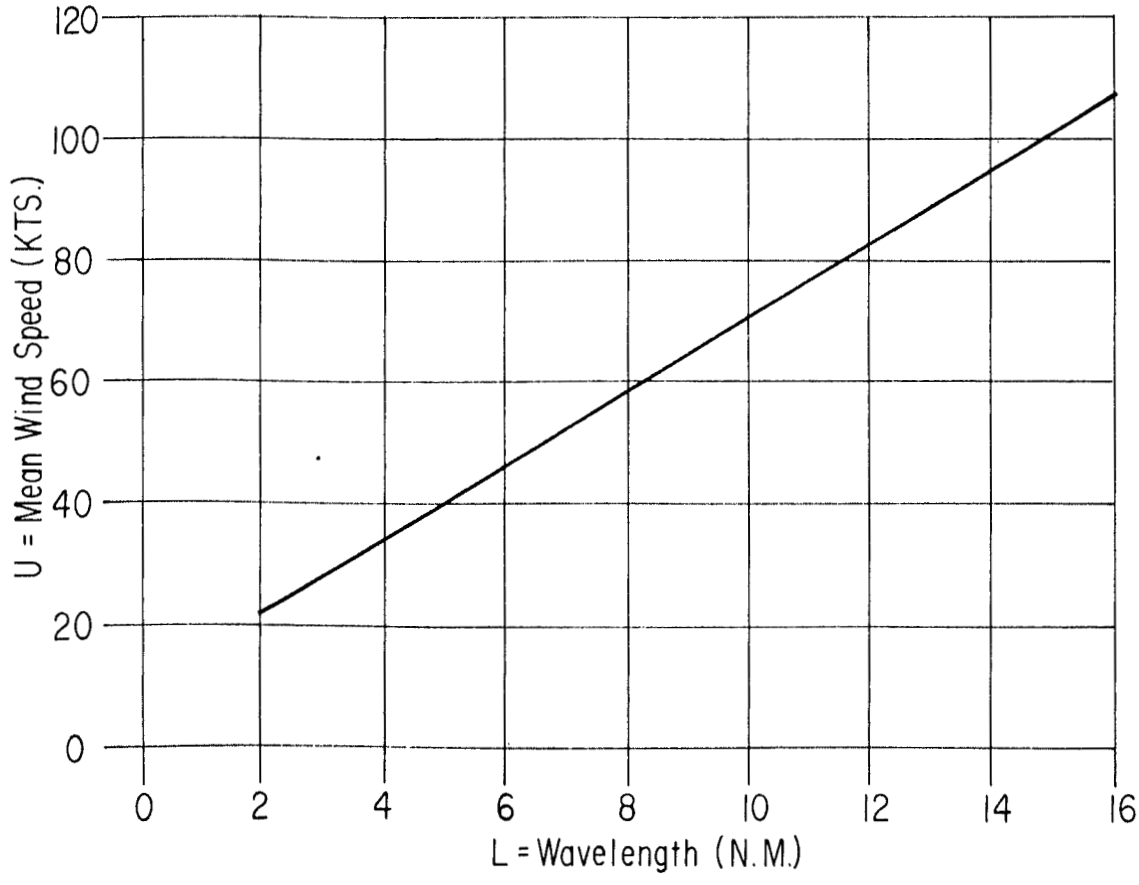

Figure 3-J-1. This graph shows the variation of mean wind speed with wavelength in the troposphere. For example, a measured wavelength (L) of 10 nautical miles indicates a mean wind speed (U) of 70 knots.

499-830 O - 73 - 2

Figure 3-J-2. Mountain wave clouds from Oregon to Utah are imbedded in a northwesterly flow that averages 89 knots from 5 to 40 thousand feet. Twelve individual wave clouds between A and B gives a wavelength (L) of 13.3 nautical miles and a calculated mean tropospheric wind speed of 90 knots.

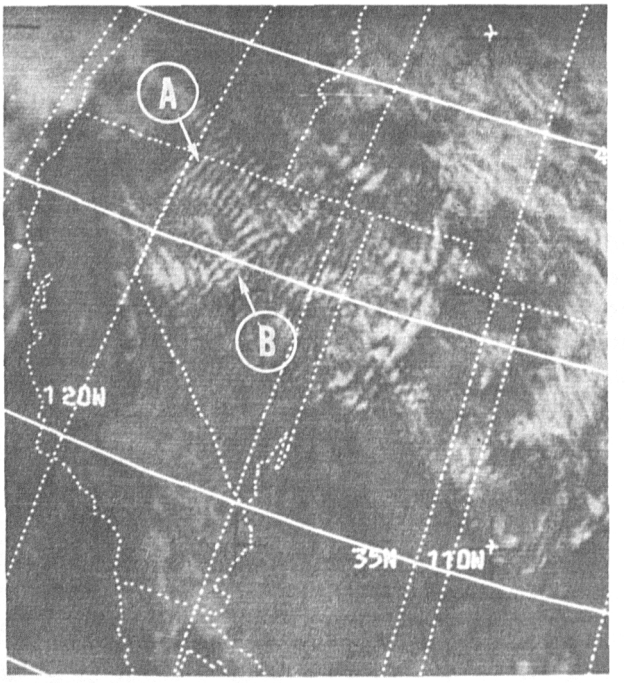

ESSA-7 1069-3 2135 GMT November 9, 1968

Figure 3-J-3. A wavelength (L) of 9.6 nautical miles for the 10 waves between A and B results in a calculated mean tropospheric wind speed of 68 knots. The observed mean tropspheric wind speed is 61 knots from 5 to 40 thousand feet. These mountain waves over and downstream of the Allegheny Mountains are in a northwesterly flow with a maximum speed of 86 knots at 36,000 feet.

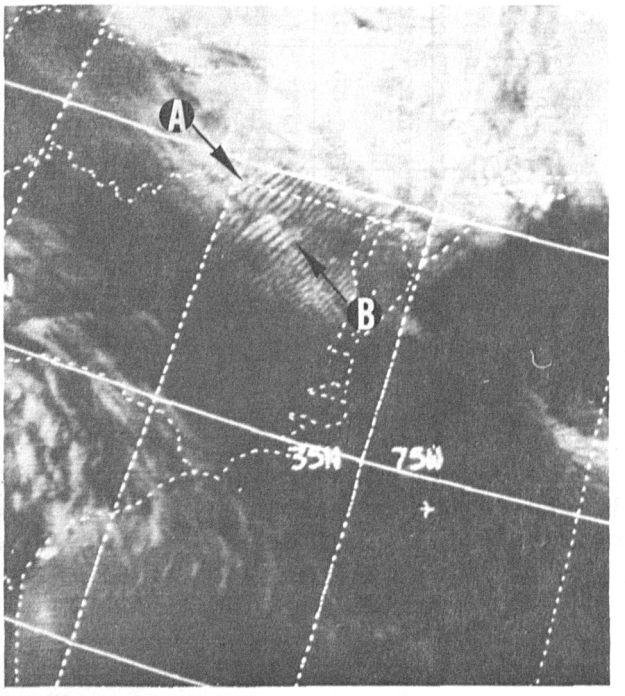

NOAA-1 1695-2 1930 GMT April 25, 1971

Chapter 5

Section B

Fog and Stratus

Introduction

A flat texture, frequently sharp edges, and patterns conforming to topographical features are the distinguishing characteristics of fog and stratus. These characteristics make fog and stratus easy to identify when it is not covered by higher clouds or is not over a snow field. When patches of higher clouds are present over stratus and fog they cast shadows that give the stratus layer a non-uniform appearance. The shadows are usually large and distinct because of the large separation between the low stratus tops and the upper clouds. It is impossible to distinguish fog from stratus in satellite photographs.

Fog, and to a large extent stratus, is formed by two physical processes: the air temperature is lowered to the dew-point temperature, or the dew-point temperature is increased to that of the air temperature. Air mass fogs form when the temperature falls; frontal fogs form in the presence of precipitation which raises the dew-point temperature (60).

Radiation fog, a type of air mass fog, is common to many continental areas. It usually occurs as a thin layer and dissipates after sunrise. Being thin, it appears gray in satellite pictures. In certain areas, radiation fog can become relatively thick and persist throughout the day. Thick fog and stratus such as this has a relatively bright appearance.

Radiation Fog

Certain areas of the world have high frequencies of fog and stratus. Fog and stratus in these areas often have characteristic shapes caused by local topography; such shapes can be used as an aid in fog and stratus identification.

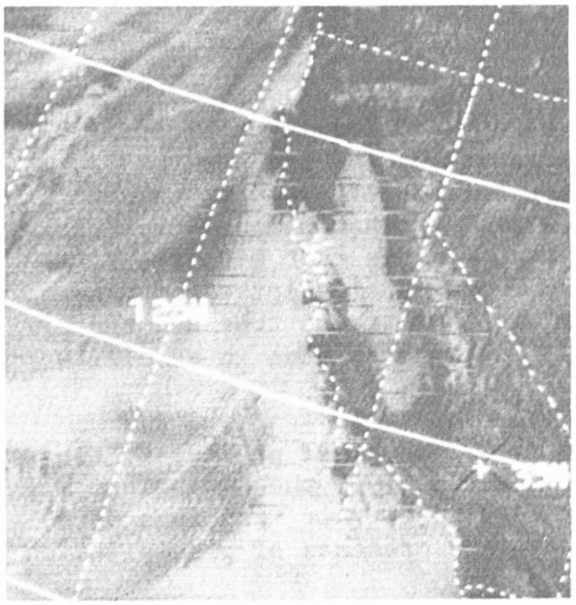

ITOS-1 4684-2 2250 GMT Feb. 1, 1971

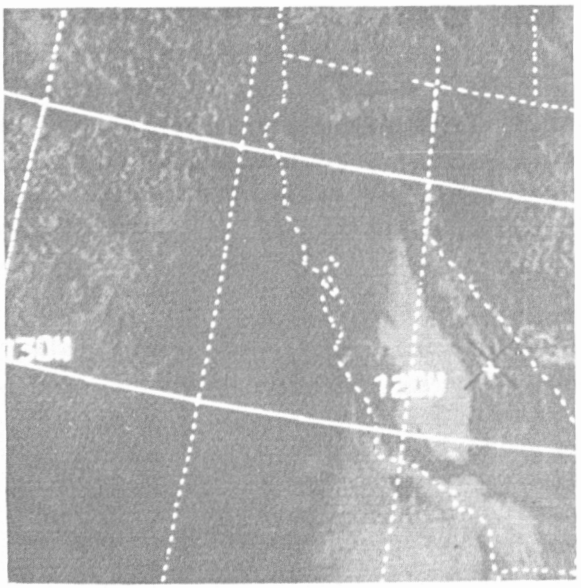

ITOS-1 4697-2 2345 GMT Feb. 2, 1971

Figure 5-B-1. This is an example of radiation fog in the Sacramento-San Joaquin Valley. The strength of the inversion and thickness of the fog layer prevented its dissipation during daytime. This fog formed during the night of January 26 and persisted through February 2. On February 1 the fog covered the entire valley westward through San Francisco Bay. On February 2 a weak cold front moved southward over the region breaking the inversion and clearing the fog in the northern part of the valley. The stratus and stratocumulus also dissipated along the coast north of the cold front.

Figure 5-B-2. This photograph shows an extensive area of radiation fog (A) over Europe north of the Alps. The southern boundary of the fog is along the foothills of the Alps and the northern boundary is along the higher terrain of southern Germany and western Czechoslovakia. The jagged edge of the southern boundary is the result of fog extending into the many valleys on the northern slope of the Alps. Other areas of radiation fog are visible at B and C.

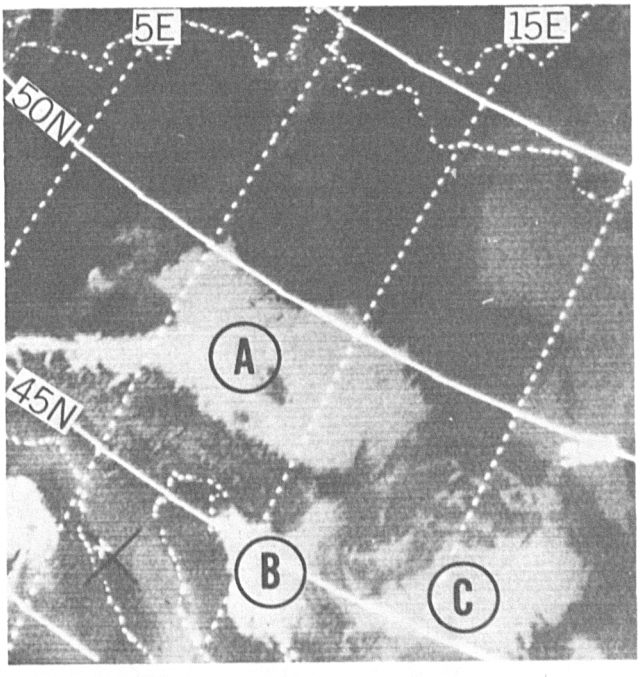

ITOS-1 3828-1 1245 GMT Nov. 25, 1970

Figure 5-B-3. This is an example of fog in the Po Valley of northern Italy (A). It is most common during late fall and winter. The eastern end of the valley opens into the Adriatic Sea. The low level winds were east or southeast and moist air from the Adriatic was being advected into the valley. Radiational cooling occurred and fog formed. The fog conforms to the shape of the valley. The fog-filled smaller valleys of the Alps and Apennine Mountains gives most of the perimeter a jagged edge.

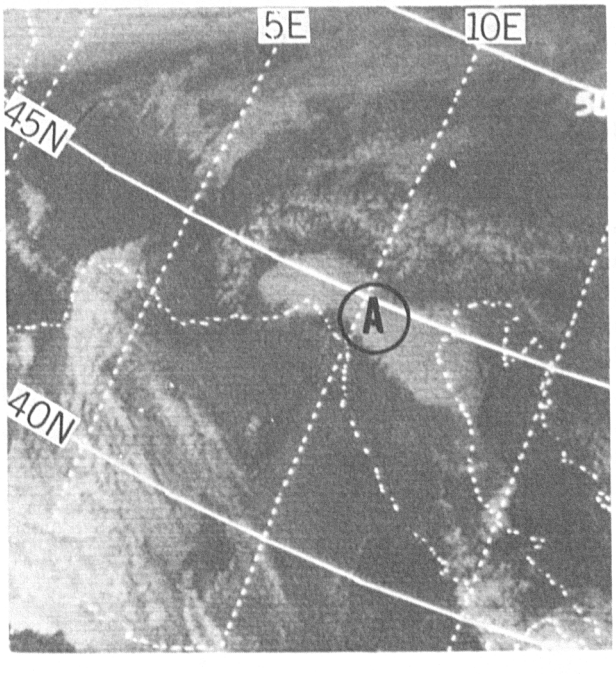

ITOS-1 3966-1 1330 GMT Dec. 6, 1970

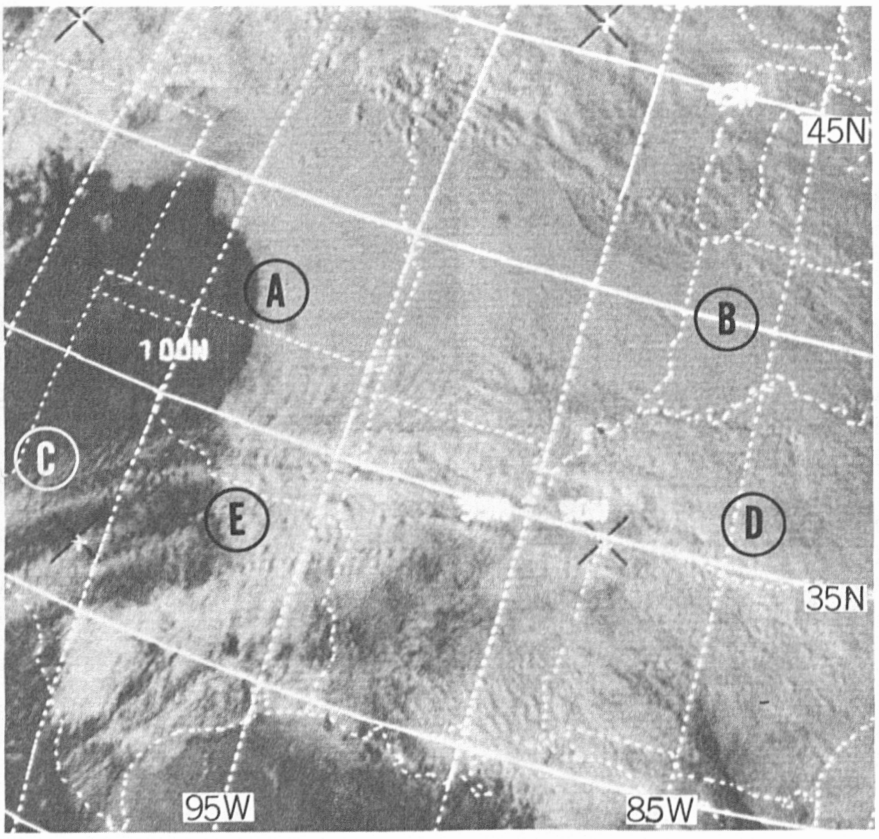

ITOS-1 4708-2 2050 GMT February 3, 1971

Figure 5-B-4. A combination of advection, radiation, and upslope cooling produced this extensive fog and stratus layer over the central United States. Ship observations in the northwest Gulf of Mexico indicate Fahrenheit water temperatures in the low 70's and air temperatures in the mid-70's. The dew-point depression was five to eight degrees. When this warm, moist air was advected northward, cooled, and lifted, fog and stratus formed. From A to B the clouds have the characteristic flat texture of fog and stratus seen in satellite photographs. The sharp edge (A) is another typical characteristic. Further south, the fog and stratus lies under cirrus associated with the subtropical jet stream (C to D). The shadows from the cirrus give this area an uneven appearance. The sharp western edge of the fog and stratus (E) can be seen through the jet stream clouds.

Figure 5-B-5. Fog and stratus covers the Sea of Okhotsk and the Pacific Ocean south and southeast of the Kamchatka Peninsula. The fog and stratus over the open water (A to B) has a characteristic sharp edge. It also terminates abruptly along the coastline on the western side of Kamchatka. The clouds extending inland across the coastline (C) are cirrus from a cluster of thunderstorms at D. The smooth, gray, somewhat mottled appearance of the formation is typical of summertime oceanic fogs. This fog and stratus formed as warmer air from Asia drifted over the water and was cooled from below.

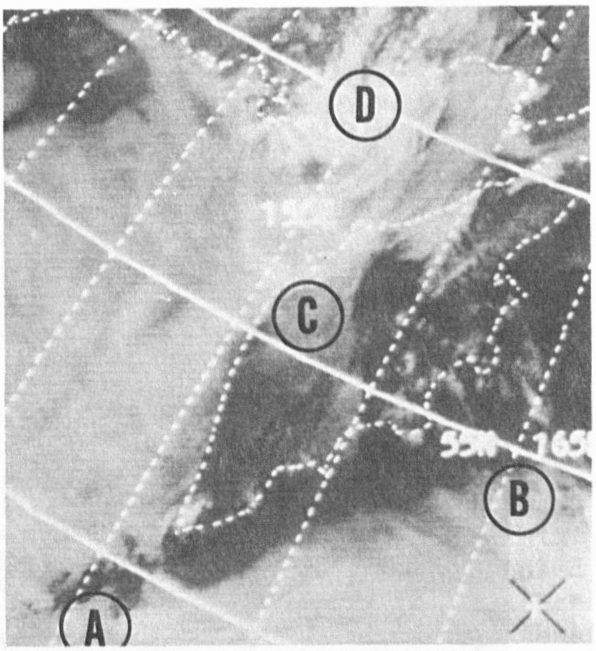

ITOS-1 2059-3 0259 GMT July 7, 1970

Figure 5-B-6. This stratus over the western Gulf of Mexico terminates abruptly along the foothills of eastern Mexico. The stratus deck has a flat texture except where some cirrus (A) casts shadows on the lower clouds.

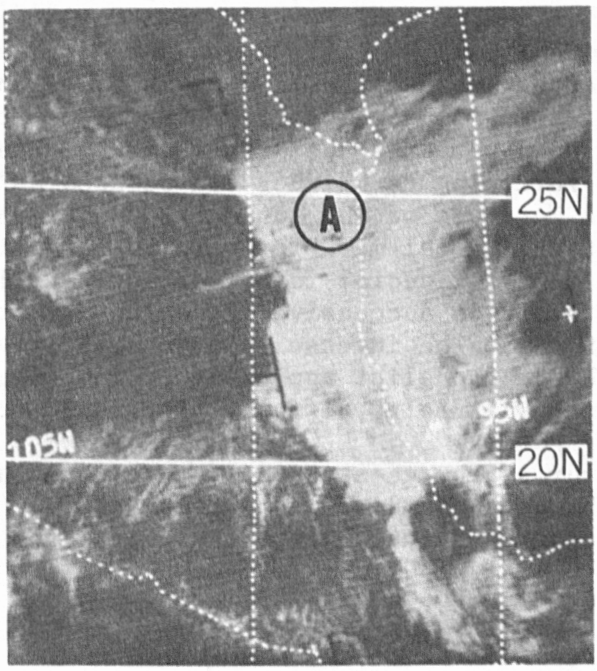

E-7 1307-4 2138 GMT November 28, 1968

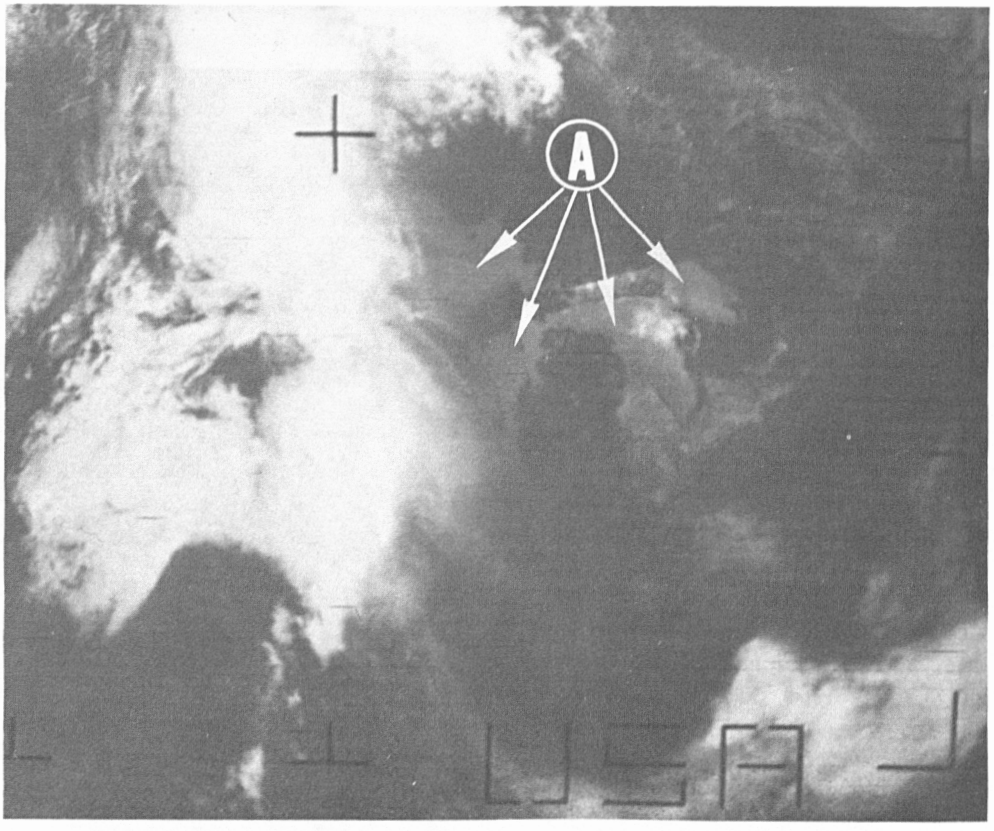

E-8 1178-8 1635 GMT July 12, 1971

Figure 5-B-7. The light gray area (A) has a smooth texture, terminates abruptly along a coastline, and contrasts with the surrounding land. This strongly suggests a fog bank over the water. Actually, the light gray area is a sun-glint on parts of the Great Lakes. (See p. 2-27, figure 2-46, this report.) The following techniques can be used as a guide for the detection and approximate location of the sun-glint. The sun-glint is to the right (east) of the center fiducial mark for morning satellite pictures and to the left (west) of the center fiducial for afternoon satellites. The sun-glint appears to move northward on successive frames on a southbound polar-orbiting satellite (ESSA-8). The inverse relationship is valid for northbound satellites (ESSA-9) with the sun-glint appearing to move southward on successive frames. The sun-glints will be at different latitudes from day to day.

Pictures from geostationary satellites have sun-glints that progress westward with the sun and are at a constant latitude throughout the day. The latitude of the sun-glint follows the sun as the seasons change.

Chapter 5

Section C

Turbulence

Introduction

The presence of turbulence can often be assessed from distinctive cloud forms which appear in satellite imagery. Lenticular cloud formations and wave cloud patterns reveal areas of orographically induced turbulence, jet stream cirrus locates regions of turbulence induced by strong horizontal shear in the upper troposphere, and convective cloud forms indicate the strength and relative depth of turbulent convection. Turbulence also occurs in certain areas of fronts, vortices, and vorticity maxima. Cloud imagery can be used to precisely locate these features and the general regions where turbulence is probable. Sometimes it is possible to assign specific turbulence intensities based on the appearance of the satellite observed cloud forms (5, 61, 62, 63, 64). It is important to remember that it is impossible to identify turbulent areas where there are no clouds or where the turbulent cloud forms are obscured by higher clouds.

The illustrations in this section are limited geographically because they were obtained from areas where a high density of aircraft reports was available. They show typical turbulence distributions in the vicinity of the cloud forms discussed. Turbulence reports plotted on the photographs are within six hours of picture time. The symbol ⩓ indicates severe turbulence, ⌒ indicates moderate turbulence, and ∧ represents light turbulence. Heights of reported turbulence are shown in hundreds of feet.

Mountain Waves

Mountain wave turbulence occurs downwind of mountains. The turbulent energy is dissipated downstream. The most severe turbulence is close to the mountains; lesser degrees of turbulence occur further downstream. Mountain wave turbulence is generally confined to altitudes below 20,000 feet. The wave clouds seen on satellite photographs are usually low or middle level clouds. Concurrent higher level turbulence, i.e., above 30,000 feet, usually can be attributed to a jet stream above the wave clouds. The intermediate levels between 20,000 and 30,000 feet have a minimum of turbulence (64, 65, 66).

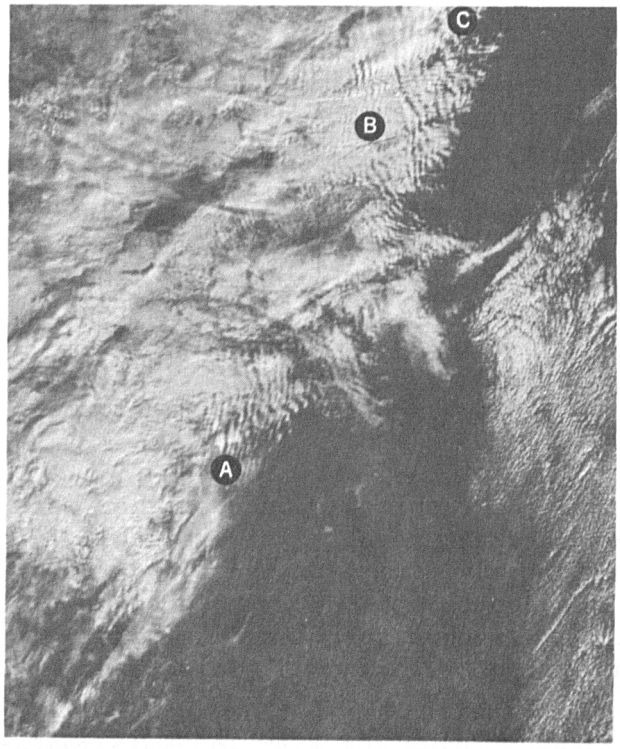

Figure 5-C-1a. NOAA-2 VHRR Visible 537-2 November 27, 1972

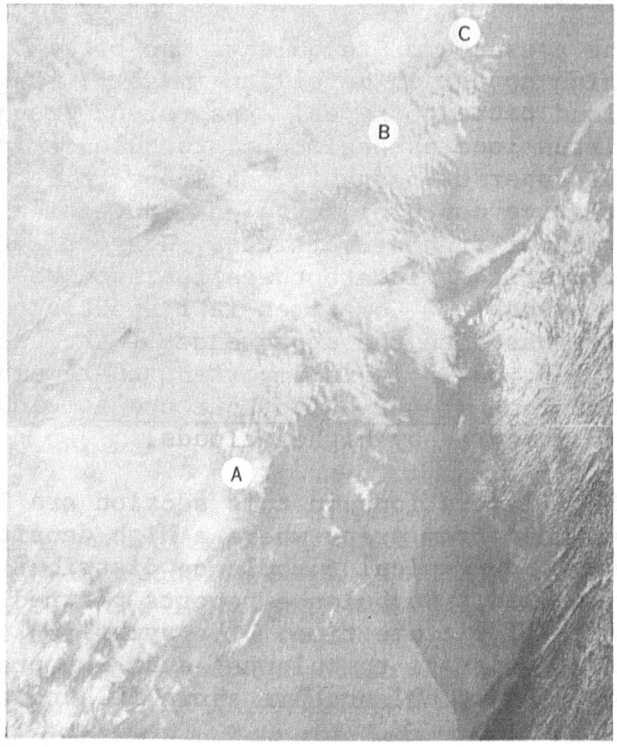

Figure 5-C-1b. NOAA-2 VHRR Daytime IR 537-2 November 27, 1972

Figures 5-C-1a and b. This example of mountain wave clouds is a simultaneous view of the clouds in the visible and infrared spectra. The mountain wave clouds exist over and to the east of the Appalachian Mountain range from Virginia, at A, and northward across the New England States to C. Resolution of these two Very High Resolution Radiometer (VHRR) photographs is about one nautical mile. At B, the interval between successive wave cloud elements is small and the cloud elements merge forming a solid deck of clouds. However, the wave crests are still distinguishable in this high resolution imagery. On lower resolution imagery the wave clouds in this area would not be discernible. When wave clouds are discernible, areas of high turbulence risk associated with the wave action can be isolated, by using the empirical rule that the turbulence is most severe close to the mountains and is less severe downwind. In this case, only light turbulence was reported above 25,000 feet. The position of the polar jet stream is off the East Coast. The severity of the mountain wave turbulence throughout the area was not reported.

Jet Streams

Except where cumulonimbus clouds are present, most turbulence of moderate or greater intensity that occurs above 30,000 feet is associated with jet streams in which strong horizontal or vertical shear is present (61, 62, 63, 64). Cirrus is often present equatorward of the jet axis on the western side of and across the top of the upper air ridges, thus permitting identification of this portion of the jet stream in satellite imagery. Turbulence occurs on both sides of the sharp edge of the cirrus shield or its associated shadow line and is generally confined to within three degrees latitude of the jet axis.

There is a higher probability of turbulence of moderate or greater intensity with dense overcast jet stream cirrus than with thin, broken, or scattered cirrus. Scattered cirrus, when seen on satellite photographs, is generally associated with light turbulence or non-turbulent conditions. Moderate turbulence is generally encountered in the top two thirds of a heavy cirrus overcast associated with a polar jet stream. The greatest probability of moderate or greater turbulence is associated with the lower two thirds of the dense overcast cirrus layer of subtropical jet streams. Light turbulence is generally found in the lower third of polar jet stream cirrus and in the upper third of subtropical jet stream cirrus (61). A higher risk of severe or extreme turbulence exists when transverse bands or cloud trails are observed near the jet than when they are not present (5, 61).

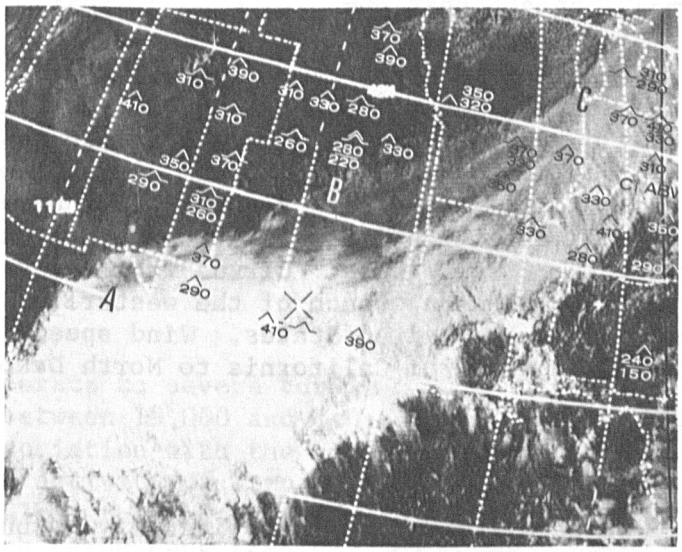

ITOS-1 3082-4 2130 GMT September 26, 1970

Figure 5-C-2. A large area of light to moderate and occasionally severe turbulence is associated with this jet stream over the central United States. This jet stream originates in the subtropics southwest of Baja California and reaches a maximum velocity of more than 100 knots over Oklahoma and to the northeast. The jet stream is located in the clear air just to the north of points A, B, and C at 200 mb. The cirrus at A and the cirrus spissatus at B originated in the subtropics and was advected northward where it merged in the main belt of hemispheric westerlies. In this case the turbulence was generally above 30,000 feet on both sides of the jet stream.

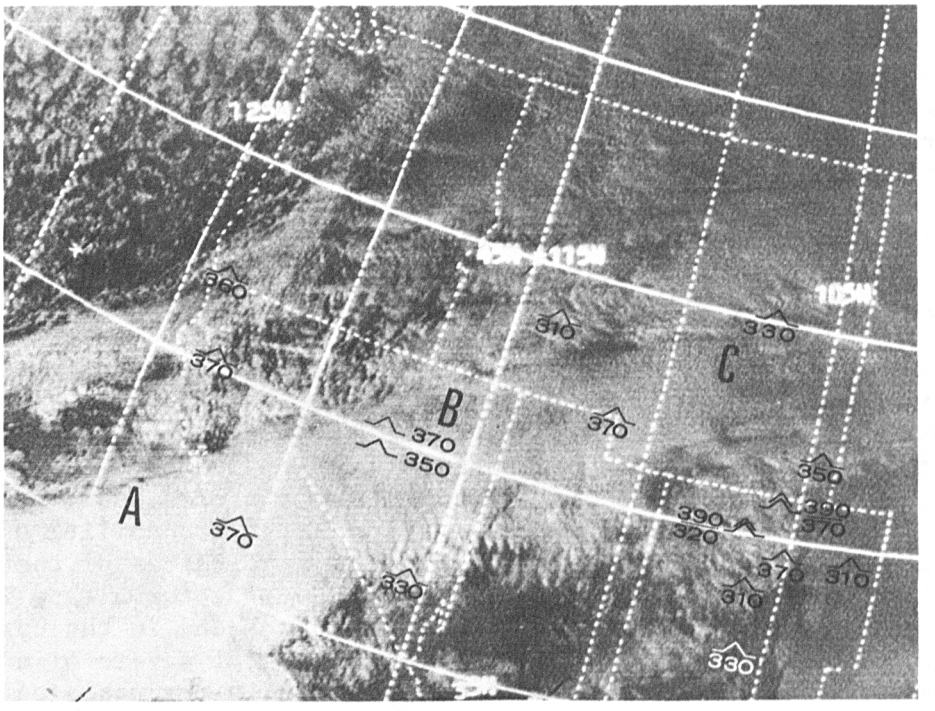

ITOS-1 3833-2 2215 GMT November 25, 1971

Figure 5-C-3. This outbreak of moderate to occasionally severe turbulence over the western United States, generally above 30,000 feet, is associated with an anticyclonically curved jet (A, B, C). A continuous shadow (B, C) appears on the lower clouds north of the jet stream cirrus. Numerous reports of light turbulence (not plotted) also were reported in the region of the jet stream. In this case, the westerlies first split over the central Pacific then merged again just west of California. Cirrus from the tropics was advected northeastward in the southern branch of the westerlies to the merge point, and then eastward over the United States. Wind speeds at 200 mb were generally in excess of 120 knots from California to North Dakota.

Convection

Convective clouds seen on satellite photographs identify turbulent areas. Cumulus and towering cumulus clouds have a typical lumpy, uneven texture and indicate the presence of light to moderate turbulence. Cumulonimbus clouds appearing either as individual cells or in clusters indicate the presence of moderate or severe turbulence. The turbulence associated with cumulonimbus clouds is not restricted to the clouds themselves, but also can occur in the clear air immediately surrounding the clouds. Significant turbulence also can occur up to 5,000 feet above developing cumulonimbus clouds (61, 64). The specific intensity of turbulence encountered by an aircraft around convective cells will vary depending on the exact location of the aircraft relative to the cloud and on the stage of development of the cloud.

The open cellular cumulus pattern frequently observed to the rear of polar fronts indicates the presence of turbulence at the low and middle levels.

As the open cells develop vertically, and take on a larger and brighter appearance, the probability of encountering more intense turbulence increases.

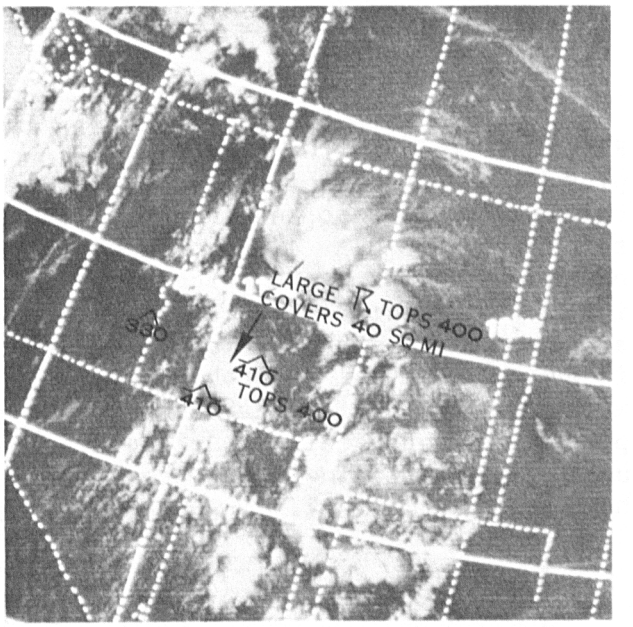

ITOS-1 2757-3 2200 GMT August 31, 1970

Figure 5-C-4. Turbulence occurs in and around convective clouds. Here, the large area of thunderstorms over the Rocky Mountains had tops near 40,000 feet. Two reports of moderate turbulence at 41,000 feet indicate that significant turbulence extends to at least 1,000 feet above these thunderstorms.

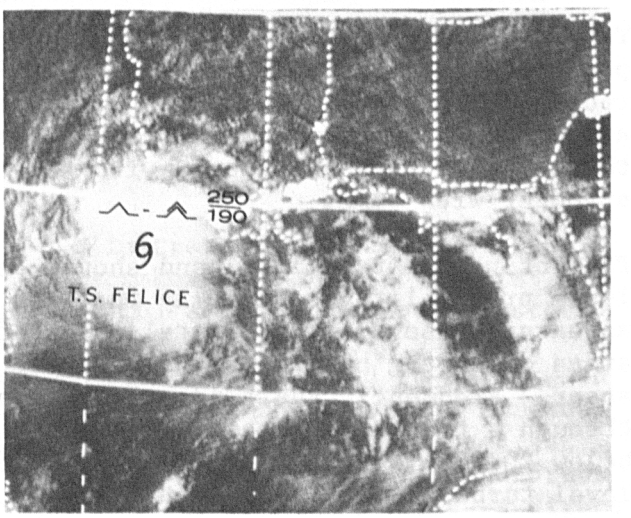

ITOS-1 2944-4 2100 GMT September 15, 1970

Figure 5-C-5. Moderate to severe turbulence occurred between 19,000 and 25,000 feet in association with the intense convective activity of Tropical Storm FELICE along the Gulf Coast. Other areas of high turbulence risk associated with convection probably occurred with the thunderstorms visible over the eastern Gulf of Mexico and Florida.

Figure 5-C-6. At the time of this picture, moderate to severe low level turbulence was reported in the vicinity of open cellular clouds. Clouds of this type form in a strong cyclonically curved wind flow to the rear of a cold front when sufficient moisture is available. This unstable air is a favored region for turbulence; the presence of open cellular clouds is useful for outlining the region of high turbulence risk.

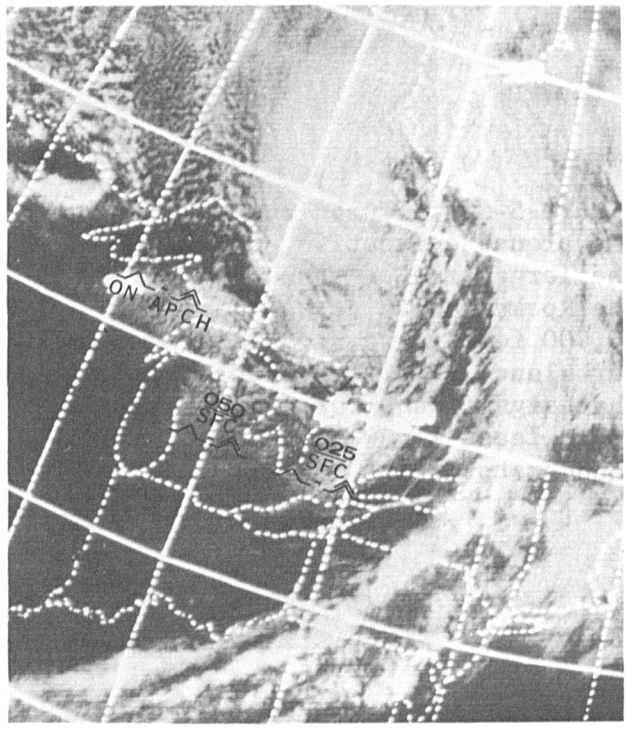

ITOS-1 2881-3 2000 GMT September 10, 1970

Other Turbulent Regions

Turbulence also is associated with fronts, developing frontal waves, and positive vorticity advection (PVA) maxima. These features have distinctive, recognizable cloud forms which make possible identification and isolation of areas where turbulence is most probable. Turbulence is most likely when the thermal gradients associated with these synoptic features are becoming stronger with time.

The entire frontal cloud band should be considered as an area of high turbulence probability, especially in areas where imbedded convective activity appears. A developing frontal wave and its associated jet stream contains areas of strong horizontal temperature gradient and strong vertical wind shear. Frequently there is a large area of significant turbulence extending through a thick atmospheric layer. In this synoptic situation, the turbulence below 20,000 feet usually is associated with the frontal clouds and the higher level turbulence is related to the jet stream (5, 63, 64).

PVA maxima, seen in satellite photographs as areas of enhanced cumulus or comma-shaped cloud patterns in the cold air behind the polar front, are associated with mid-tropospheric short-wave patterns and are areas of probable turbulence. The favored area for turbulence is the northeast quadrant of PVA maxima.

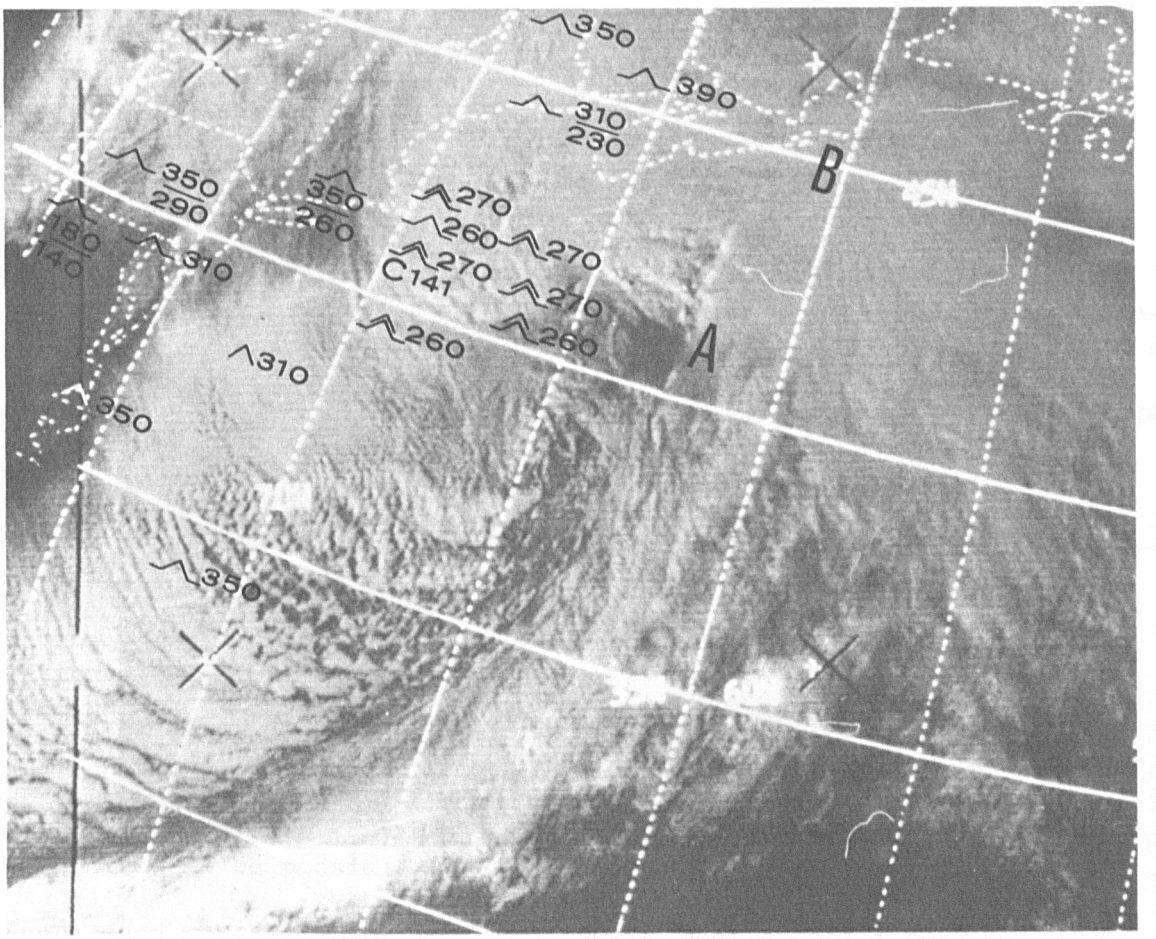

ITOS-1 4219-2 1900 GMT December 26, 1970

Figure 5-C-7. This figure and figure 5-C-8 illustrate the turbulence associated with two major East Coast storms. The December 26 storm (above) is fully occluded (1800 GMT, central pressure 957 mb) and the December 31 storm (figure 5-C-8) is still an open wave (1800 GMT, central pressure 998 mb). Most of the severe turbulence with the above storm was reported to be between 26,000 and 27,000 feet, to the north and somewhat to the west of the surface low center, and to the west, or poleward of the anticyclonically curved jet stream cirrus (A to B). Light and moderate turbulence extended many hundreds of miles through a deep layer of the atmosphere along the East Coast--a direct result of the thermal and wind shear patterns associated with this major storm.

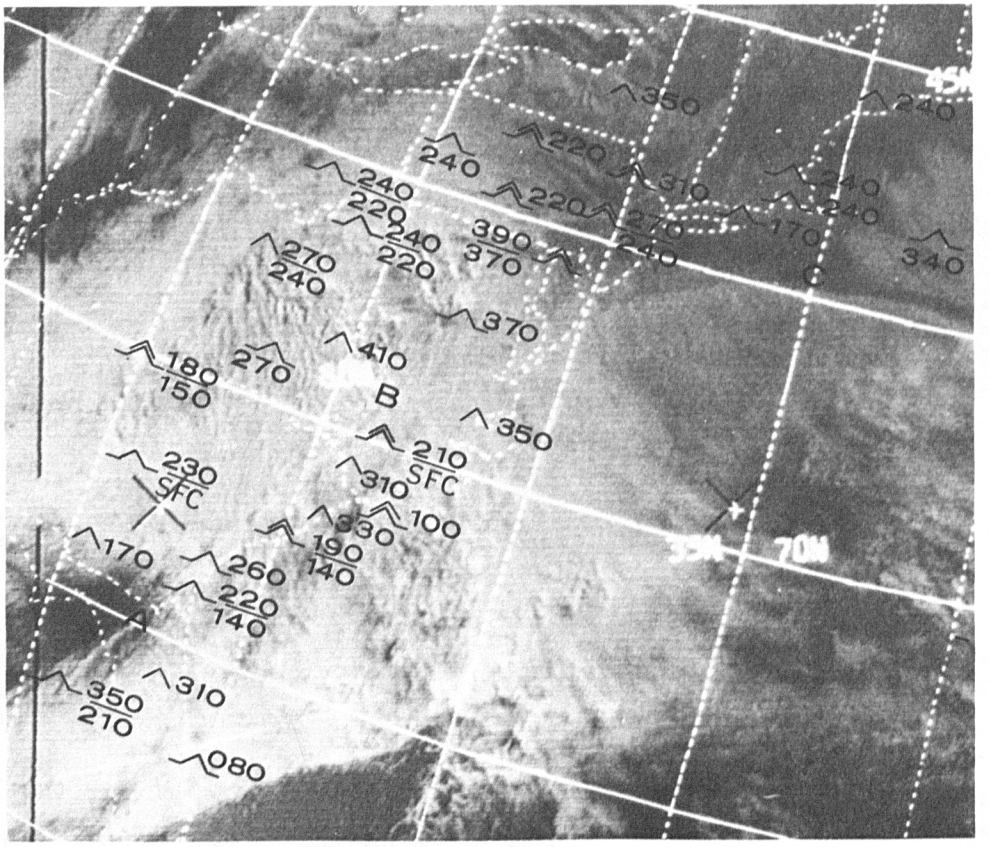

ITOS-1 4282-2 1900 GMT December 31, 1970

Figure 5-C-8. There were numerous reports of moderate and severe turbulence with this major storm in the high air traffic areas of the East Coast. As in the December 26 storm, most of the turbulence was reported poleward of the jet stream (A, B, C). Again the turbulence extended through a deep layer of the atmosphere from the surface to well above 30,000 feet.

This storm and the one in figure 5-C-7 illustrate how one can associate turbulent areas with particular cloud patterns. By using satellite pictures to locate major storms, one can infer wind shears and thermal patterns favorable for the production of significant turbulence and can identify turbulent areas not only in data-rich areas, but also in data-sparse areas.

Chapter 5

Section D

Mesoscale and Subsynoptic Scale Vortices

Introduction

Frequently, small-scale spirallike cloud patterns appear in satellite photographs. These patterns may exist at any cloud level. This section will discuss those occurring in the lower cloud layers, primarily because they are observed most frequently. These small-scale spirallike cloud patterns range in size from the mesoscale (10 to 100 n.mi.) eddies, which occur downwind from island barriers, to the subsynoptic scale (100 to 300 n.mi.) spiral patterns which occur in stratocumulus clouds adjacent to coastlines. Small vortices or eddies also are observed within the large areas of fog that occur under oceanic highs, as well as in cumulus fields of polar air masses.

As with the study of many mesoscale cloud patterns, the observation and investigation of subsynoptic scale vortices was facilitated by the advent of satellite photographs. The detection of small-scale vortices by means of conventional synoptic data is extremely difficult because vortices of this size are too small to show up in the "wide mesh" standard weather-observation network, and normally are too large to be recognized by ground observers (67). As operational satellite imagery with a resolution of one mile or less becomes available, it will be possible to detect local scale eddies (1 to 10 n.mi.).

Subsynoptic and mesoscale vortices should not be confused with those of a larger scale since they are generally formed by different mechanisms and do not represent a potential for development. Small-scale vortices can affect the local cloud distribution when they occur in areas of local, short-range forecast interest. These patterns also give insight into the wind field in data-sparse regions.

499-830 O - 73 - 3

Mesoscale Vortices in Stratocumulus

Mesoscale eddies occur most often in the stratocumulus field on the eastern side of a subtropical high downwind from mountainous islands. These eddies are most often seen in the satellite photographs downwind from the Canary Islands, the Cape Verde Islands, Madeira Island, and Guadalupe Island. The conditions necessary for development of these eddies are a strong low-level inversion which caps the stratocumulus field, an island barrier that pierces the inversion, and a persistent low-level wind flow in the 10- to 25-knot range. If the wind speed exceeds 25 knots, the eddy pattern will tend to break down, and, if the wind speeds are less than 10 knots, the eddies usually will not form. Ideally, mesoscale vortices are shed from alternating sides of an island, one spiraling to the right, the other to the left. After forming, the eddies move downwind with the surrounding air flow. The eddies will persist until the flow pattern or the inversion changes, or until the region of influence of one eddy overlaps and counteracts the motion of a neighboring eddy of an opposite circulation (67).

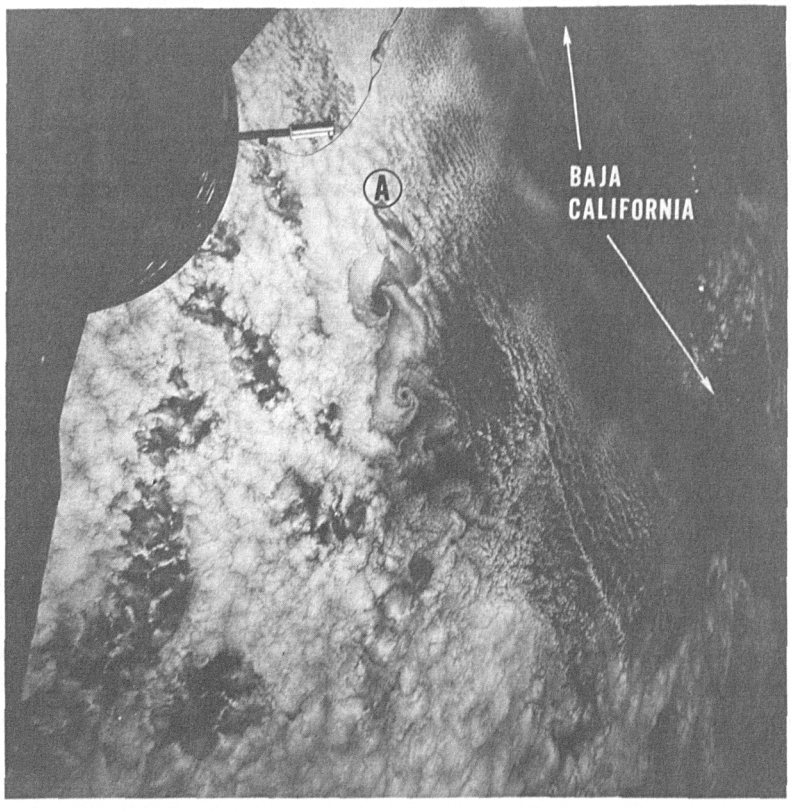

Figure 5-D-1. A Gemini XII picture of mesoscale eddies that developed downwind of Guadalupe Island (point A). The eddies formed in the dense stratocumulus cloud deck that dominated the eastern side of the subtropical high. Note the detail of the eddies visible from this low altitude (153 mi.) photograph.

Gemini XII Orbit 30 Frame 108 November 13, 1966

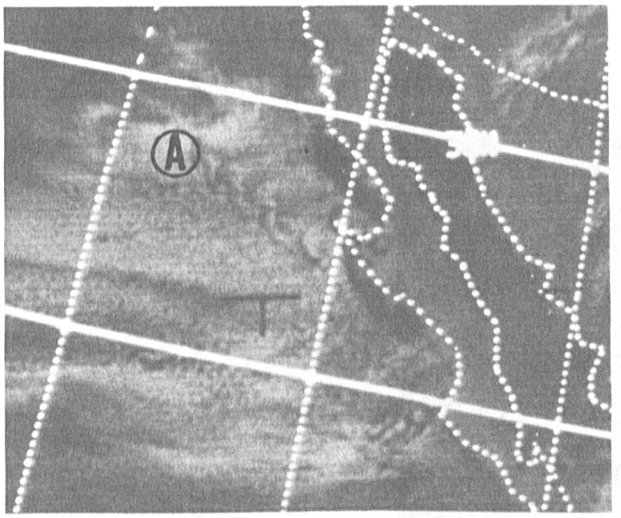

Figure 5-D-2. An eddy pattern extending 200 miles downwind from Guadalupe Island (A), viewed from an altitude of 900 miles. In this example the eddies are embedded in the stratocumulus cloud deck associated with the subtropical high off the west coast of the United States. The eddies extend southeastward from the island, indicating a persistent northwest low level wind flow.

ESSA-9 2842-5 2149 GMT October 11, 1969

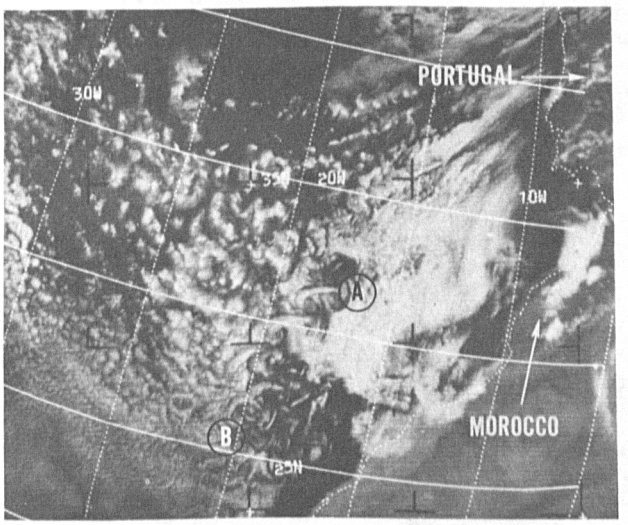

Figure 5-D-3. An eddy pattern extends downwind from Madeira Island (point A). The eddies extend approximately 400 miles to point B, indicating that the synoptic situation of the area has remained stable for at least 24 hours. These eddies formed in the stratocumulus cloud deck on the eastern side of the subtropical high in the western North Atlantic.

ESSA-9 1627-5 1522 GMT July 6, 1969

Mesoscale Vortices in Cumulus Clouds

Mesoscale spirallike cloud patterns are frequently observed in the cumulus cloud field poleward of polar fronts east and southeast of the Kamchatka Peninsula, the Kuril Islands, Japan, and Greenland. These patterns can vary in size from mesoscale to synoptic scale and form in the cyclonic flow associated with a surface or low level vortex or trough. The primary cause of these patterns is horizontal shear in the low levels that results in cyclonic twisting of the cloud pattern. In addition, the patterns seem to occur when the atmosphere aloft is extremely cold and the winds are light. The vortices may or may not be located downwind of a land barrier.

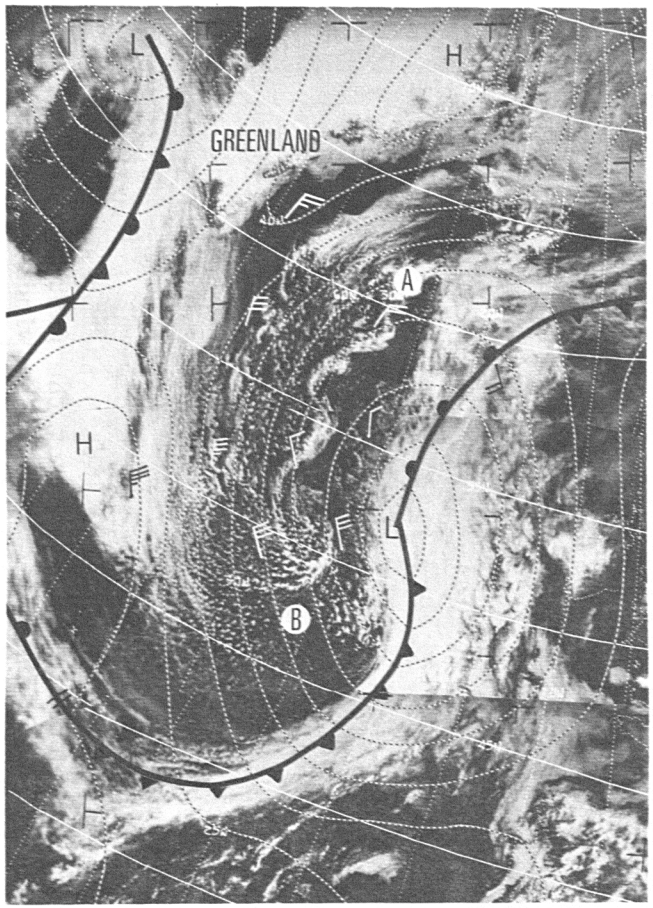

Figure 5-D-4a. ESSA-9 1352-3,4 June 14, 1969. Surface Analysis 1200 GMT June 14, 1969.

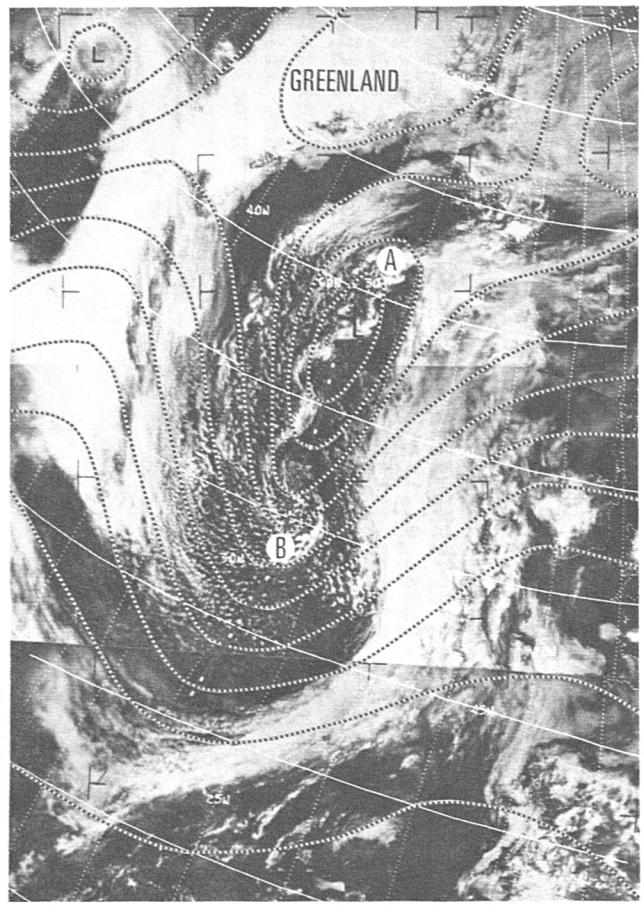

Figure 5-D-4b. ESSA-9 1352-3,4 1350 GMT June 14, 1969. 500-mb Analysis 1200 GMT June 14, 1969.

Figures 5-D-4a and b show an example of a mesoscale spirallike cloud pattern southeast of Greenland (A to B). The pattern in this situation was caused by the cyclonic shear in the low-level wind field and is reflected in the cumulus cloud field. The pattern also lies along or just to the west of a high amplitude mid-tropospheric trough line. The surface winds shown in figure 5-D-4a are for 1200 GMT on June 14, 1969.

Mesoscale Vortices in Fog

Mesoscale vortices or eddies are observed frequently in the fog or stratus areas associated with stationary or quasi-stationary oceanic highs. In general, the winds are light at the surface and at the low levels in the region where the eddies form. Even though the winds are light, there is sufficient horizontal shear in the wind field to create the eddy pattern. Such horizontal shear may or may not be due to a land barrier.

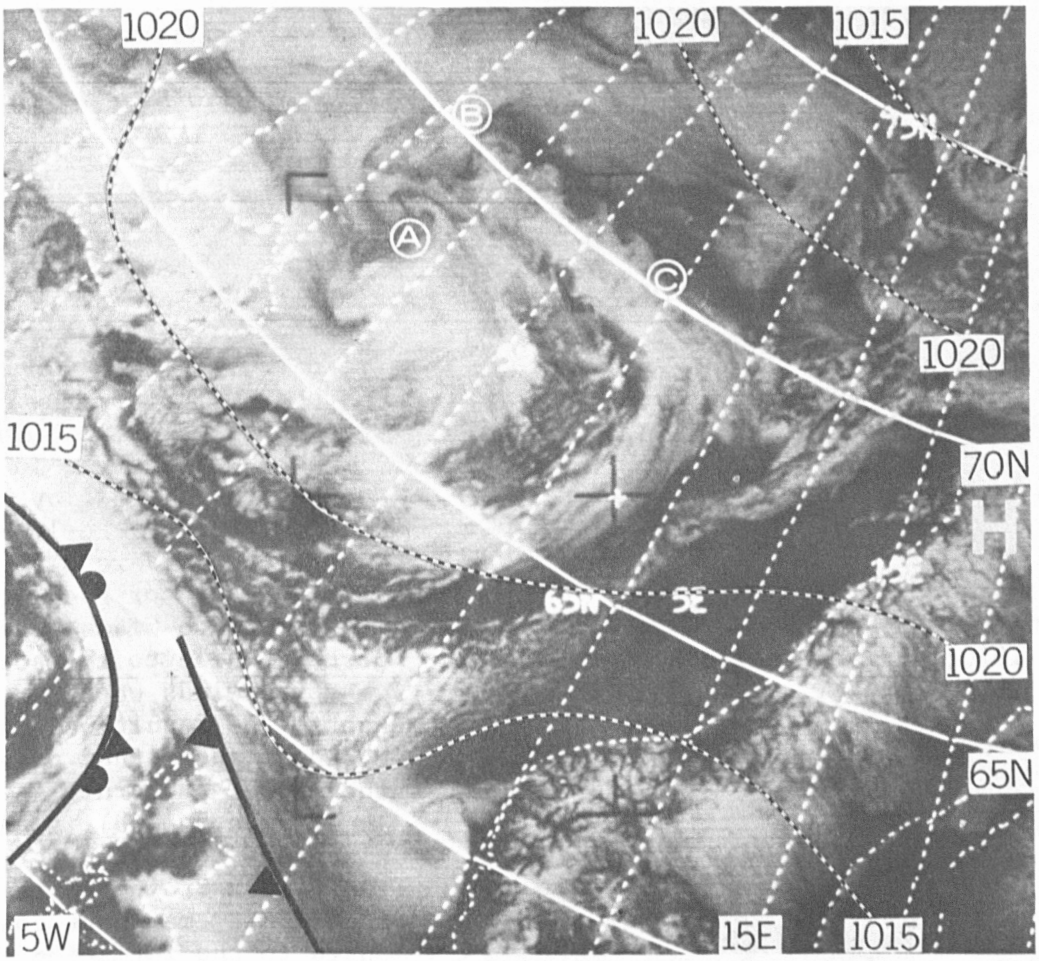

ESSA-9 5535-2 1226 GMT May 15, 1970
Surface Analysis 0700 GMT May 15, 1970 Berlin Weather Chart

Figure 5-D-5. In this photograph, at A, B, and C, are examples of mesoscale vortices or eddies that appear in fog and stratus areas associated with stationary or quasi-stationary oceanic highs. The area is dominated by a quasi-stationary high pressure cell with the main center over Greenland. Fog and stratus is the predominant cloud type in the region of the eddies. The surface analysis shows the very flat pressure-gradient across the region on May 15, 1970; thus, light surface winds can be inferred. The eddies exist in this area of light winds. The eddies from B to C have formed along or just equatorward of the shear zone associated with the surface ridge line.

Subsynoptic Scale Vortices

Subsynoptic scale vortices form, as do other types of eddies, as a result of horizontal shear in the surface or low-level wind field. This shear can be induced on the wind field dynamically or orographically. Subsynoptic scale vortices or eddies usually are seen in the cumulus cloud field poleward of a polar front, or in stratocumulus clouds adjacent to coastlines.

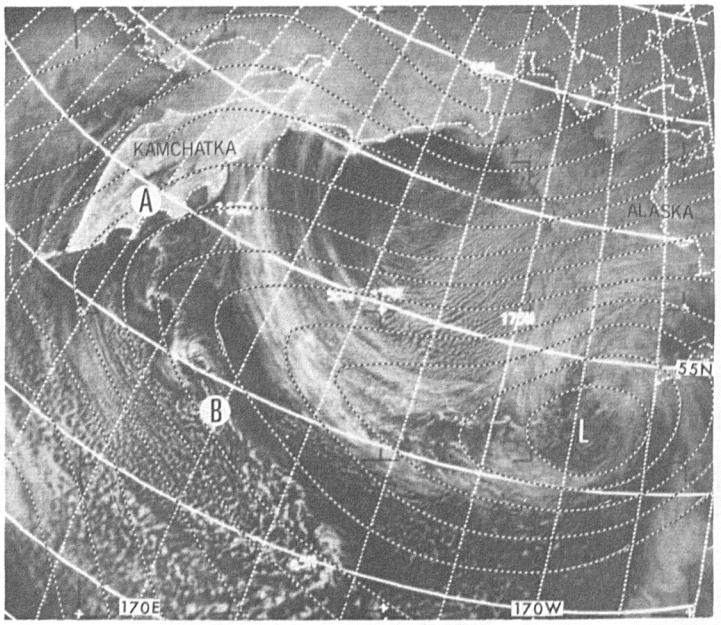

Figure 5-D-6a. ESSA-9 4705-2 0136 GMT March 10, 1970; Surface Analysis 0000 GMT March 10, 1970.

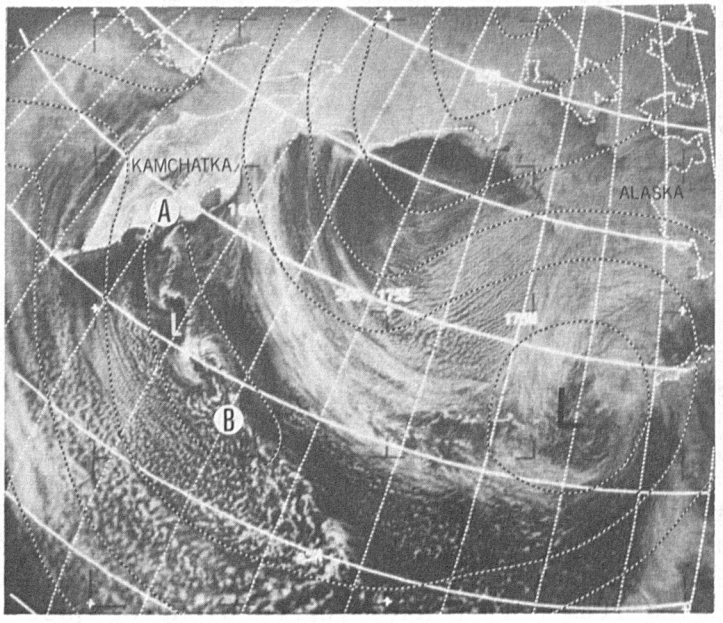

Figure 5-D-6b. ESSA-9 4705-2 0136 GMT March 10, 1970; 500-mb Analysis 0000 GMT March 10, 1970.

Figures 5-D-6a and b. A subsynoptic scale vortex train extends from A to B, southeastward from the Kamchatka Peninsula. The vortices were formed in the cumulus cloud field by cyclonic shear in the low-level wind field (figure 5-D-6a). In the region of the vortices, light surface winds were reported, while to the southwest the winds were 20 to 30 knots; the result was the cyclonic shear that created the vortex pattern. At 500-mb (figure 5-D-6b), a narrow, elongated cold low overlies the vortex train. This factor also may have contributed to the formation of the vortices.

The subsynoptic scale vortex or eddy pattern that forms in the Atlantic Ocean west of the Mediterranean Sea is an example of the type of eddy that occurs in stratus or stratocumulus clouds adjacent to coastlines. This subsynoptic scale eddy is observed less frequently than those which form in subtropical highs or cumulus cloud fields. The formation of this eddy pattern is a result of orographically induced cyclonic shear in the low levels. This region of cyclonic shear exists at the mouth of the Mediterranean Sea when the synoptic scale wind flow from the north and east first traverses the higher terrain of the Iberian Peninsula. When conditions are favorable for low-level cloud formation, the eddy pattern will appear on the satellite photographs. This pattern will remain stationary and will persist as long as conditions are favorable for its formation.

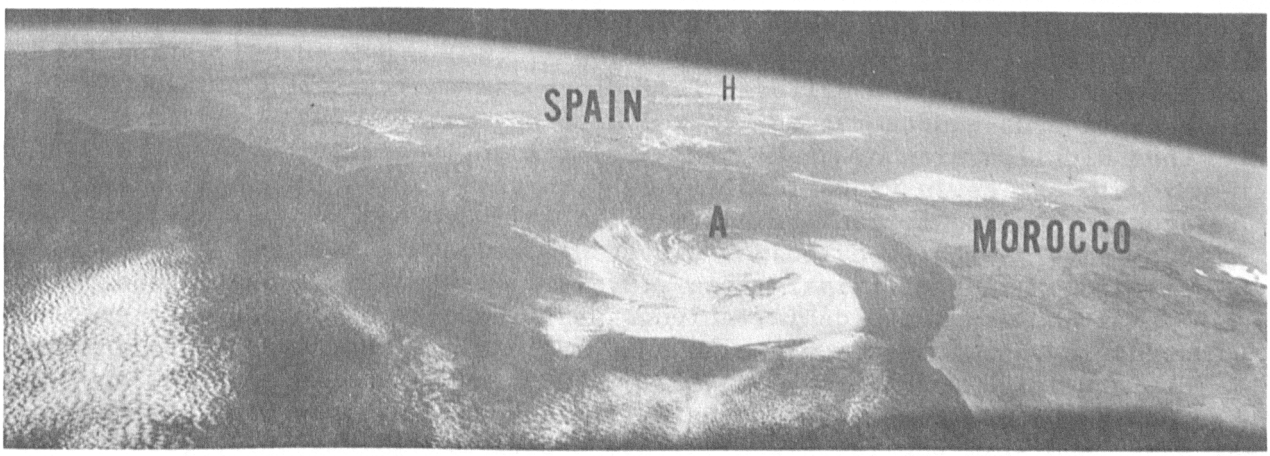

Figure 5-D-7a. Gemini X Orbit 26 Frame 28 July 20, 1966

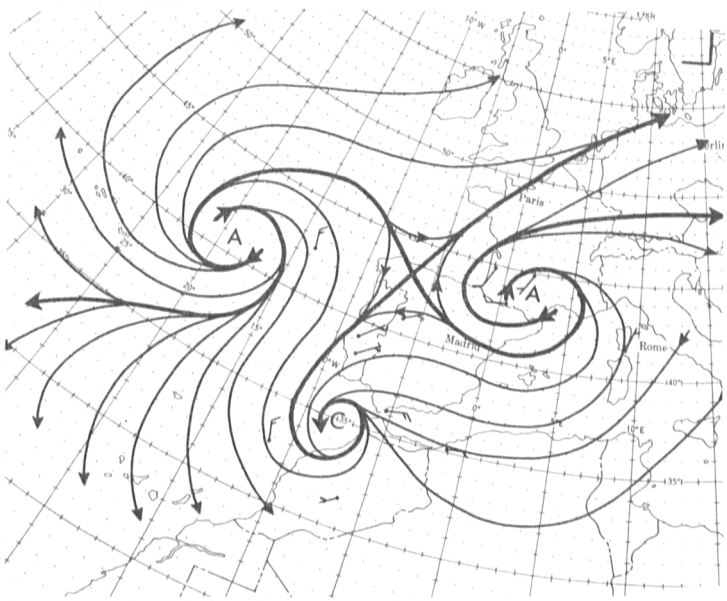

Figure 5-D-7b. Surface Streamline Analysis 0600 GMT July 20, 1966

Figures 5-D-7a and b. This is an example of the subsynoptic scale eddy that forms at the mouth of the Mediterranean Sea (figure 5-D-7a). Cyclonic shear in the region of the eddy pattern was caused by both the northerly and the easterly wind flow (figure 5-D-7b). Note that the pattern consists of a single eddy and not a group of eddies as in previous examples. The streamline analysis is based on the surface winds for 0600 GMT on July 20, 1966.

Chapter 5

Section E

Severe Weather

Introduction

Specific atmospheric conditions accompany the occurrence of severe weather, particularly tornadoes (68). Usually, a severe weather watch is issued several hours in advance of the severe weather event and identifies a large area (usually 120 by 240 miles) in which severe weather is expected to occur. Combined use of imagery from meteorological satellites and conventional data yields a better assessment of the behavior of the atmosphere than is possible with the use of conventional data alone; this leads to more reliable and accurate warnings of severe weather. Satellite imagery gives the viewer an immediate feeling for the dynamics of a severe weather situation. Synoptic and mesoscale features, important in severe weather development, are readily detectable in satellite imagery. Visible and infrared imagery from polar-orbiting and geostationary satellites provide valuable information for: (1) locating the active squall line (the area of maximum severe weather threat); (2) locating the low-level jet (850-mb) and the axes of the polar and subtropical jets; (3) determining vertical wind shear between the lower and upper troposphere; (4) locating the area where the low-level and mid-level jets intersect (the major axis of latent tornado activity) and (5) isolating small (15 miles square) areas of immediate tornado threat; these areas are located by the combined use of satellite imagery, the surface wind field, and radar information.

Squall Lines

In most cases convectively unstable squall lines form along the convergent low-level streamline which separates warm, moist, maritime air from warm, dry, continental air; this air mass boundary is the so-called "dry line". An excellent example of a dry line in the process of becoming an active squall line is shown in figure 5-E-6c.

> "...these so-called "dry lines" may remain quasi-stationary for days...without becoming active; but under certain conditions, they appear to act as mechanisms aiding the formation of large thunderstorms and organized squall lines...this is most likely when a supporting feature...exists at 500 mb" (69).

Most severe weather occurs in the area of deep, moist convection which is associated with this boundary.

The squall line appears in satellite imagery as a line of cumulonimbus clusters which have merged together to form a bright band. The threat of severe weather is greatest in the area where the squall line takes on a characteristic tapering shape in the imagery (figure 5-E-1). The narrowing of the line to the south should be expected since the preferred region of the squall line for new storm formation is its southernmost portion. Here the smaller, less mature storms are located; while the older, more mature storms are further north (70).

Locating the 850-mb Wind Maximum

The axis of the low-level jet parallels an active squall line. Its exact location beneath the squall line cloud shield depends on the curvature of the low-level flow and the isotach field. However, if the axis is assumed to be near the back edge of the active squall line clouds and its direction parallel to the squall line, its location will be very close to the actual position.

Middle and Upper-Level Jets

An important factor in forecasting severe weather is the presence of a mechanism that produces upper-level divergence. In most cases this is a jet stream. The locating of jet streams from satellite imagery has been discussed in Chapter 3 of this Technical Report.

The polar jet stream has long been recognized as an important factor in the development of severe weather. Miller (68) has pointed out that the major activity in a tornado outbreak will be located near the intersection of a low-level and upper-level jet. The axis of the polar jet stream can be either south (figure 5-E-2) or north (figure 5-E-3) of the region in which severe weather occurs.

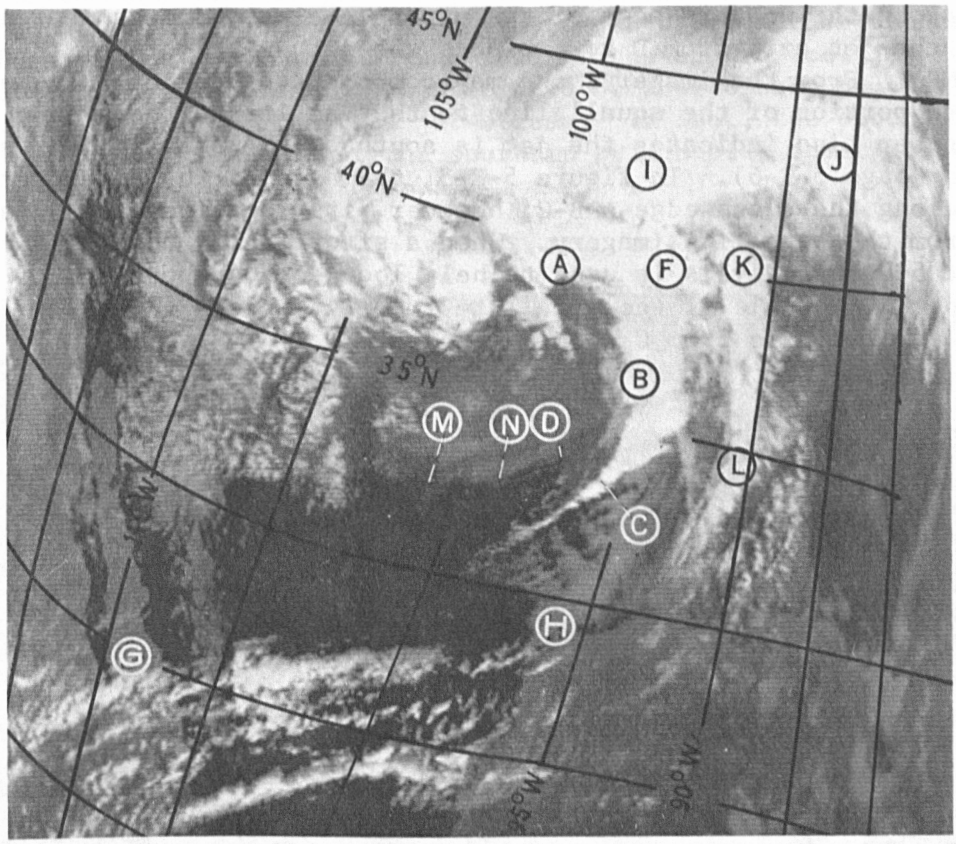

NOAA-1 Daytime Infrared 2125 GMT February 18, 1971

Figure 5-E-1. This figure is a classic example of an infrared picture received during a severe weather outbreak. The tapering cloud system, with its back edge extending from A to B to C, is associated with an active squall line and represents the area of maximum severe weather threat. Four tornadoes were reported near A between 1930 GMT and 2210 GMT, one near B at 2045 GMT, and three near C between 2055 GMT and 2335 GMT. The 850-mb jet axis is parallel to the squall line; in this case it is within the convective cloudiness from C to F. The axis of the polar jet stream at 500-mb extends along the cloud edge M-N-D. The subtropical jet is easily detected from its cloud shield which extends from G to H; however, in this case, the polar jet stream was the dominant triggering mechanism in the severe weather outbreak. High clouds associated with a warm front extend from I to J, and a band of cirrus (remnants of the convection on February 17, 1971) from K to L.

In figure 5-E-2, the axis of the polar jet is easy to locate along the cloud edge B-C-D. The presence of the jet is also indicated by the anticyclonic curvature along the western edge of the upper-level cloudiness near A. Extension of the jet axis from D to A places the jet axis south of the squall line (Q'LINE). From the imagery, one may compare the vertical wind shear at the southern portion of the squall line to that at its northern end; the change in shear also indicates the jet is south of the squall line (shear is discussed on page 5-E-6). In figure 5-E-3, the axis of the polar jet is easy to locate along the cloud edge A-B-C; however, its location past C is not apparent from the satellite imagery. When a situation of this kind occurs, the current 500-mb analysis is used to help locate those portions of the jet which are not detectable in the satellite imagery; in the case of figure 5-E-3, the extension is from C to E.

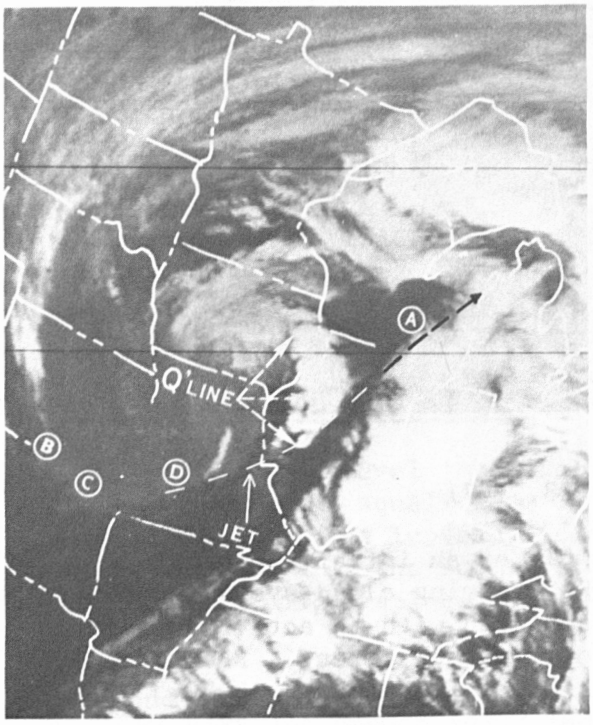

NOAA-1 Daytime Infrared 2026 GMT
February 19, 1971

Figure 5-E-2. A squall line (Q'LINE) extends from eastern Iowa through western Illinois. Tornadoes were reported in the southern end of the squall line between 1935 GMT and 2100 GMT.

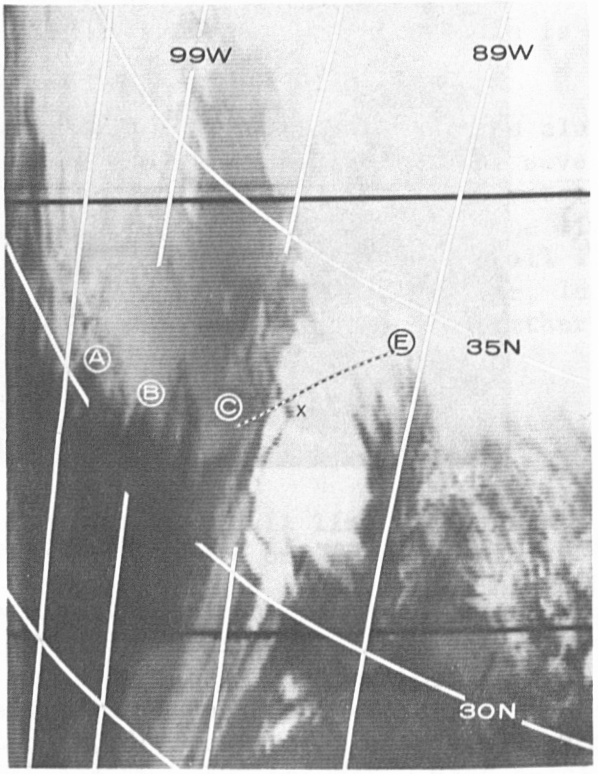

NOAA-1 Daytime Infrared 2016 GMT
February 21, 1971

Figure 5-E-3. Mississippi tornadoes began at 2100 GMT near X, beneath the intersection of the low and mid-level jets.

The subtropical jet stream has been found to play a key role in a large number of severe weather outbreaks (figure 5-E-4). Tornadoes occurring in the presence of the subtropical jet stream are normally beneath its intersection with the squall line and to the north of the jet axis. Prior to the availability of satellite observations, the role of the subtropical jet in severe weather situations was not fully appreciated because of the paucity of data along the path of the subtropical jet stream. In fact, the subtropical jet may well have been mistaken for the southern branch of a split polar jet during some severe weather outbreaks.

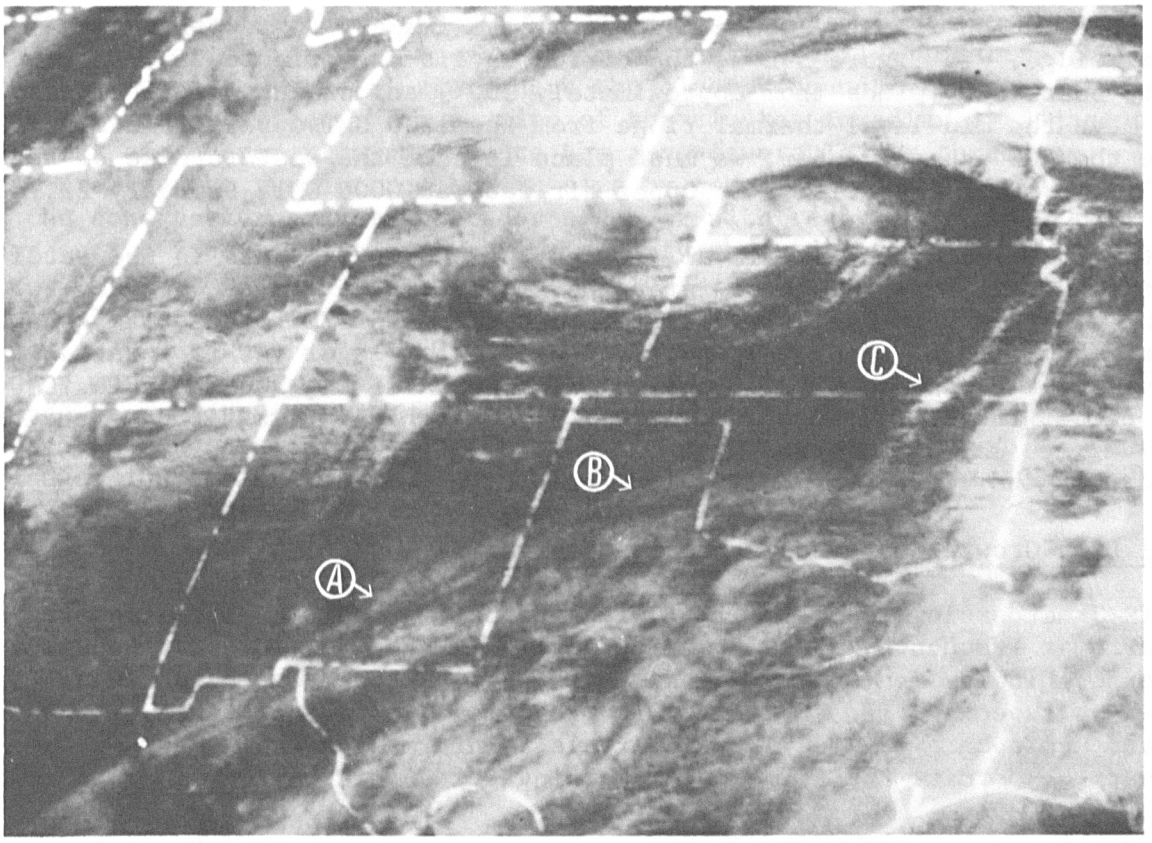

ATS-3 Frame 29 2016 GMT May 5, 1971

Figure 5-E-4. The axis of the subtropical jet stream is made apparent by the anticyclonically-curved cloud shield that extends from A to B. Extrapolation of the jet from several consecutive ATS pictures (or extension from just one picture) showed that the main axis of the subtropical jet would intersect the north-south oriented squall line (C) that is forming in eastern Kansas and northern Oklahoma. Several devastating tornadoes occurred beneath this intersection. The May 5, 1971 outbreak is described in detail later in this section of Chapter 5.

Detection of Shear

Convective clouds building through a shearing current are stretched out horizontally so that the elongated axis of the anvil is parallel to the direction of the vertical shear. In most severe weather situations, when thunderstorms develop in a strong shear environment, their anvils will extend to the right of the squall line and will be parallel to the vertical wind shear between the lower and upper troposphere. Since the vertical wind shear vector between the lower and upper troposphere is parallel to the mid-tropospheric isotherms, it is possible to use satellite imagery to locate the mid-tropospheric thermal ridge, a place where the maximum instability often occurs. This is done by using the thermal patterns from the current mid-tropospheric analysis and the shear orientation from the subsequent satellite imagery to reposition the thermal ridge. In figure 5-E-3, the cirrus anvils are oriented from northwest to southeast (winds from approximately 300°) across the squall line. If we move the mid-level thermal ridge from the 1200 GMT upper air analysis to fit the 300° shear vector, we must place it near the western edge of the squall line; this is verified by upper air data at 0000 GMT, February 22, 1971.

From the location of the low-level jet and the 500-mb jet axis in the satellite imagery, it is possible to infer the amount of veering between the two. Veering of winds with height is an important parameter in forecasting severe weather (68). In figure 5-E-3, the axis of the low-level jet is located parallel to the western edge of the squall line while the 500-mb jet axis extends across the squall line from C to E. Using this information, a veering of 40 degrees may be inferred; the 0000 GMT analysis for February 22, 1971 showed that the winds turned from 190° at 850 mb to 235° at 500 mb.

Squall Line Growth Characteristics as Observed by ATS-3

The ATS-3 meteorological satellite, with its ability to view the same area of the earth at frequent intervals during daylight, provides information valuable for use in issuing severe weather warnings. During days when severe weather is expected, the spacecraft is programmed to take pictures of the Northern Hemisphere at 11-minute intervals. Information from these frequent observations permits the issuance of warnings of severe weather in mesoscale detail.

Cumulus cloud formation along the dry line is often observable in satellite imagery up to two hours prior to the time it becomes a squall line sufficiently active to be detected by radar. This squall line predecessor cloud formation first appears as a long thin line in the satellite imagery. Next, small areas of convective cloudiness begin to form along the thin line, organize into clusters as they grow, and form the initial stages of an active squall line. These intense thunderstorm complexes can remain active for several hours and interact vigorously with their surrounding environment. They are readily identified by the subsidence zones surrounding them. The subsidence zones appear as narrow gray areas within the squall line cloud band. In the initial stages of squall line development, clear areas usually surround the entire complex. Later as the thunderstorm complex grows and interacts with its environment, its anvil clouds may overlap other clouds and merge with other complexes; however, each individual complex usually makes its presence known by developing some clear areas around its periphery. When tornadoes

occur, they are located in the low-level inflow region of a complex; hail, however, may occur anywhere within a complex.

Isolation of Threat Areas

It is possible to isolate very small areas of immediate tornado threat from satellite imagery, radar, and surface wind field data; the method is graphically demonstrated in figures 5-E-5 (a-d). To locate immediate tornado threat areas, first identify the boundary of each individual convective cluster along the squall line. Second, draw a streamline analysis of the surface wind field to define the asymptote of convergence in the low-level streamline field (this will usually parallel the back edge of the active squall line) and mark the area of low-level inflow into the thunderstorm complex. Lastly, identify the area on the inflow side of the cluster where the cluster boundary and the asymptote of convergence intersect. The portion of the cluster immediately adjacent to this point of intersection represents the area favorable for tornadoes. The threat area can be further reduced in size by comparing the moist inflow region with the echo patterns from the radar scope or with radar echo lines as they appear on the facsimile radar chart. Identify the radar echo within the cluster which is associated with the moist inflow region. The area of this echo near its tapered end represents the smallest threat area that can be defined. As a rule, the threat area should not cover more than one-half of a radar echo or enter more than 15 miles into its boundary. Once identification of a threat area has been made, its movement should be forecast from cell movement on radar. If possible, successive ATS pictures should be used since the complexes undergo changes in time which can alter the threat area patterns; this occurred in the May 5, 1971 example which is discussed next.

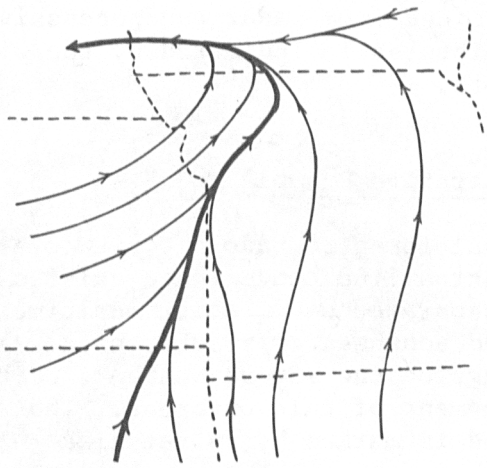

Surface Streamline Analysis 2300 GMT May 5, 1971

Figure 5-E-5a. Melding this analysis with the satellite picture to the right makes it possible to identify the low-level inflow region of each complex, marked with a dot in the picture.

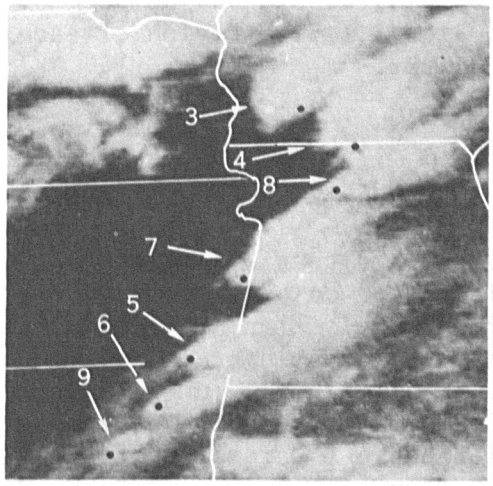

ATS-3 Frame 41 2256 GMT May 5, 1971

Figure 5-E-5b. There are seven active convective clusters within this squall line (numbered 3 to 9 for continuity with the next section). The portion of each complex favorable for tornadoes is marked with a dot.

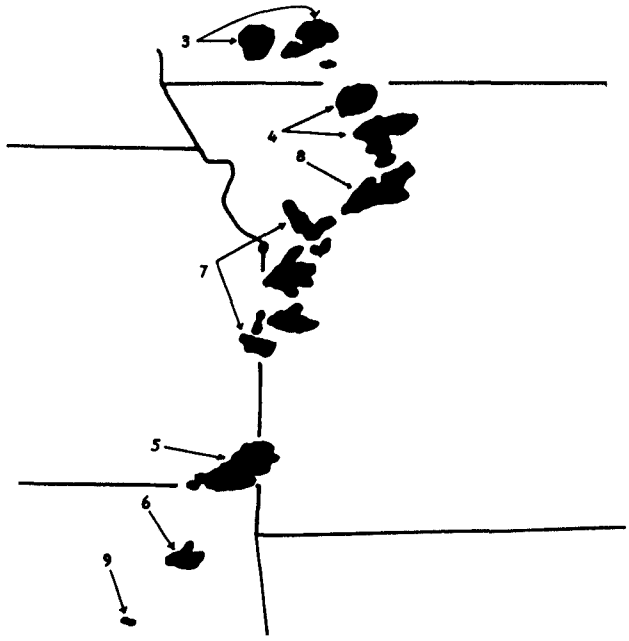

Radar Echoes 2256 GMT May 5, 1971

Figure 5-E-5c. Arrows point to the radar echoes which make up the thunderstorm clusters in figure 5-E-5b. An area which is one-half the echo size or 15 miles, whichever is less, should be isolated at the low-level inflow region of each echo cluster.

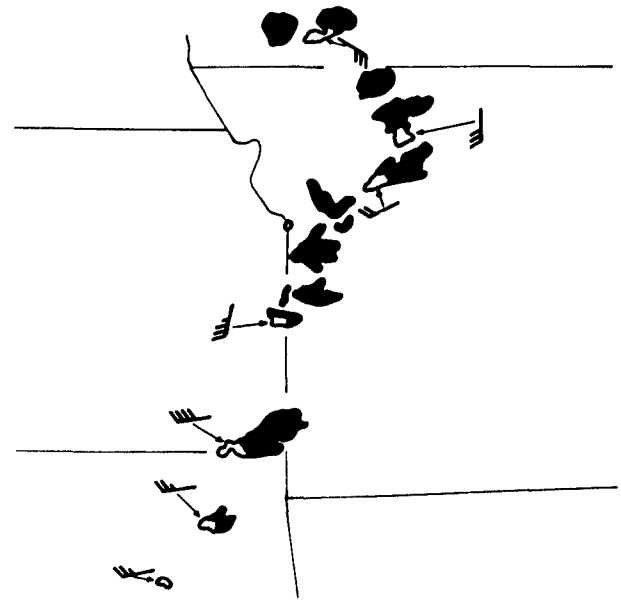

Tornado Threat Areas 2256 GMT May 5, 1971

Figure 5-E-5d. The tornado threat areas (shown above as white portions of the echoes) are isolated by integrating the information in the three previous figures. The expected movement of each threat area as determined from radar and successive ATS pictures is indicated by the wind vectors.

The Tornado Outbreak of May 5, 1971, An Illustrative Example

The synoptic situation on May 5, 1971 was ideal for a tornado outbreak over the midwestern United States. Considerable streamline convergence existed at the lower levels along the "dry line" which separated warm, moist maritime air and warm, dry continental air. A well defined southwesterly subtropical jet intersected the highly unstable area and triggered the severe weather. Figures 5-E-6 (a-q) show the step-by-step development of this outbreak. The location where a tornado or tornadoes occurred is marked by an asterisk (*) on each figure.

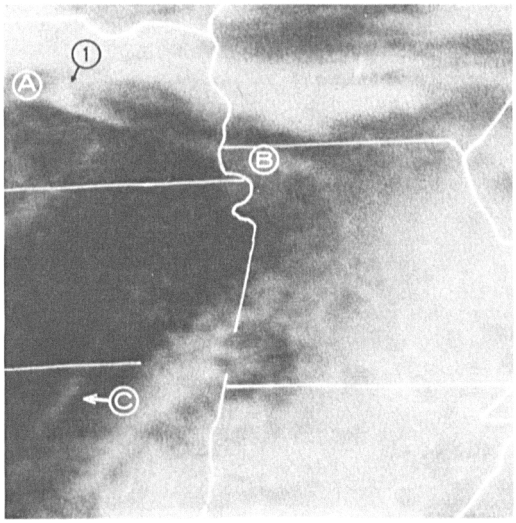

ATS-3 Frame 21 1833 GMT May 5, 1971

Figure 5-E-6a. Convective activity has just become apparent at point 1 along the line A-B. Cloudiness has just become visible at C along the dry line. It was nearly 2½ hours before the line B-C was detected by radar and identified as an active squall line.

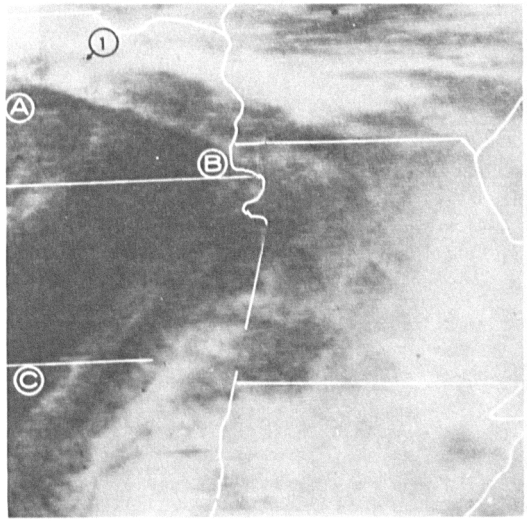

ATS-3 Frame 23 1858 GMT May 5, 1971

Figure 5-E-6b. Cloudiness along the dry line B-C is more evident. The thunderstorm complex at 1 bears watching; notice the clearing around it. The low-level inflow region of 1 should be identified as an area with a high potential for tornadoes.

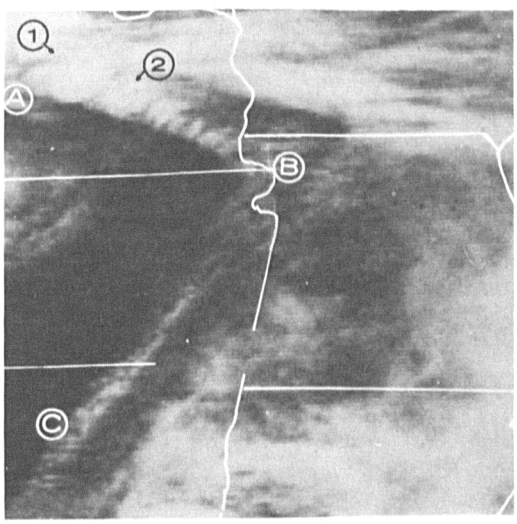

ATS-3 Frame 27 1951 GMT May 5, 1971

Figure 5-E-6c. A second thunderstorm complex has formed on A-B at 2. The danger of tornadoes at 1 still exists. Cloudiness along the dry line is now well defined. The area around C is where the major tornado activity should be expected; here the line is intersected by the subtropical jet (see figure 5-E-4).

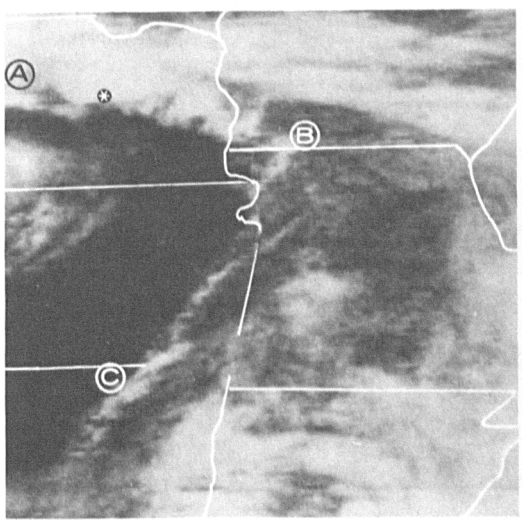

ATS-3 Frame 30 2027 GMT May 5, 1971

Figure 5-E-6d. Convective activity has increased along the dry line near C. The thunderstorm complexes at 1 and 2 have grown in size and are merging. Tornadoes were reported (as indicated by asterisk) between 2025 GMT and 2030 GMT.

499-830 O - 73 - 4

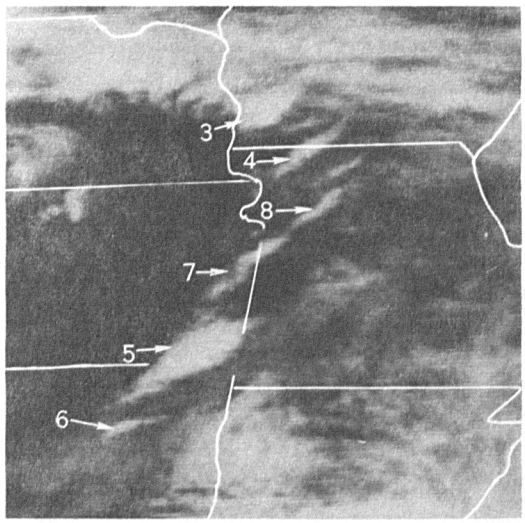

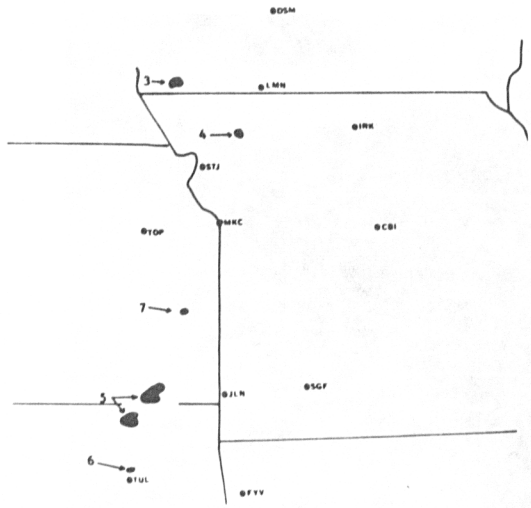

ATS-3 Frame 33 2109 GMT May 5, 1971 Radar Echoes 2109 GMT May 5, 1971

Figures 5-E-6e and f. There are six distinct thunderstorm complexes visible in the ATS imagery along the dry line. The storm complex at 3 can be traced back nearly an hour, the complex at 4 and the large complex at 5 can be traced back for nearly 50 minutes, the storm complex at 6 has been in existence for about 40 minutes, and the clusters at 7 and 8 have been going for 25 minutes. The squall line has just begun to take shape in the radar presentation.

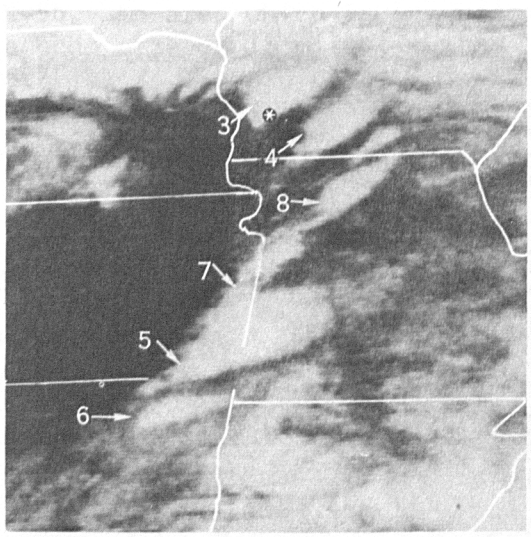

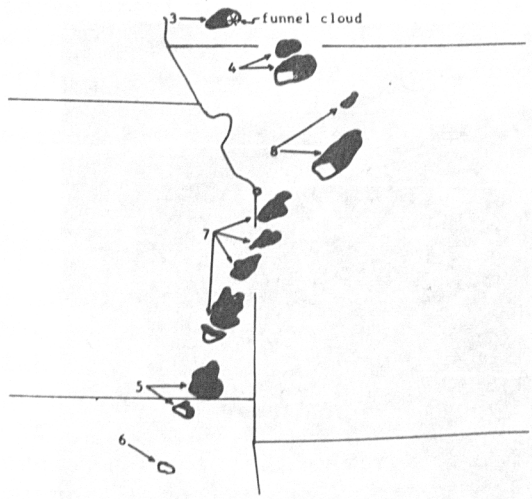

ATS-3 Frame 36 2147 GMT May 5, 1971 Radar Echoes 2147 GMT May 5, 1971

Figures 5-E-6g and h. The squall line shows up very clearly in both the satellite imagery and the radar. The clear portions of the radar echoes represent the tornado threat areas which were located using the method previously described. The only tornado activity reported near picture time was a funnel cloud (*) at 2150 GMT beneath cluster 3.

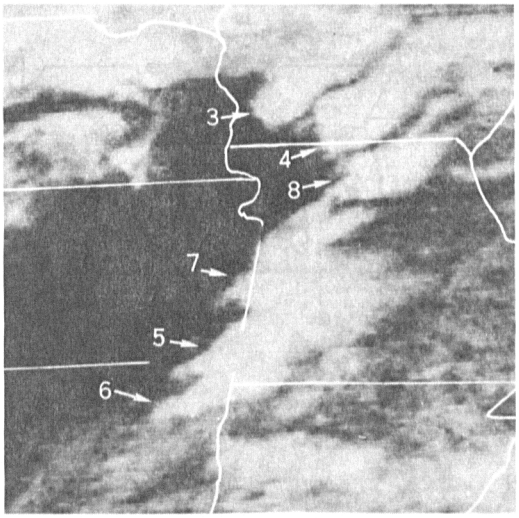

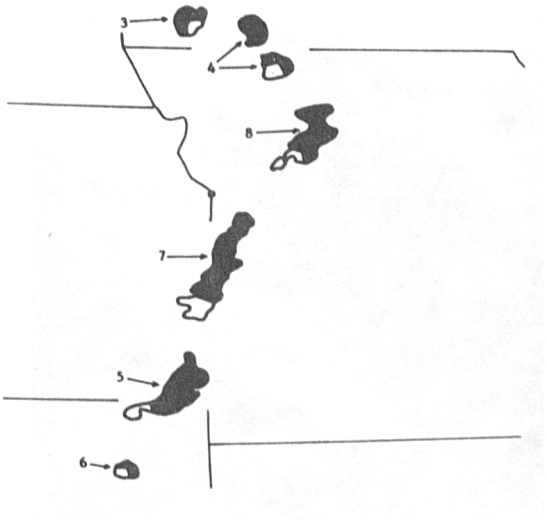

ATS-3 Frame 39 2229 GMT May 5, 1971 Radar Echoes 2229 GMT May 5, 1971

Figures 5-E-6i and j. All of the storm complexes are easily located in the satellite imagery and radar. The white portions of the radar echoes represent tornado threat areas. Notice the bulge in complex 4 at its northwestern corner; this is associated with the northern echo in that cluster which is moving to the west on a collision course with complex 3. A junction actually occurred as the northern echo in cluster 4 changed complexes and became the new threat area in complex 3 (see radar in figure 5-E-61). The same type of split also is occurring in complex 8, which will transfer the northern portion of its echo to complex 4.

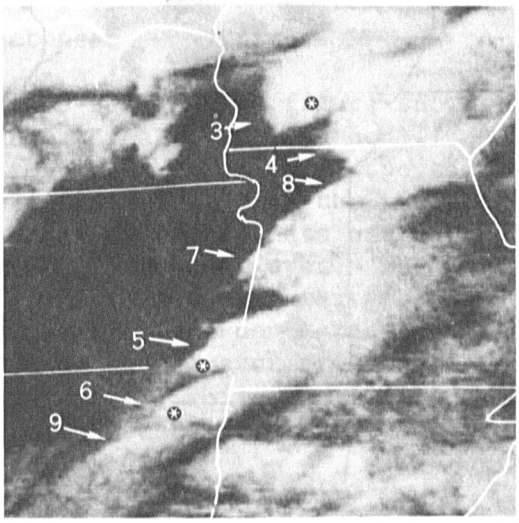

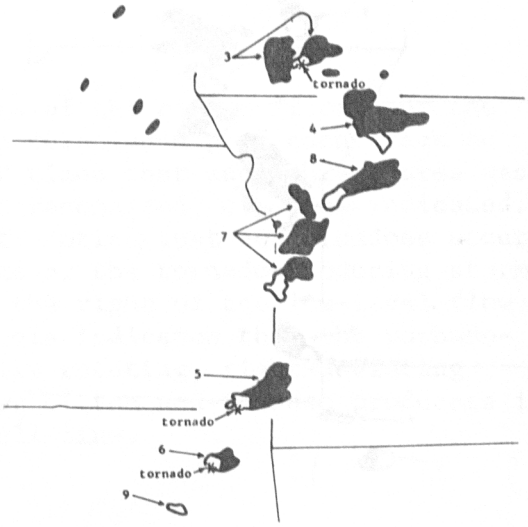

ATS-3 Frame 42 2307 GMT May 5, 1971 Radar Echoes 2307 GMT May 5, 1971

Figures 5-E-6k and 1. The echo transfers mentioned above are apparent in both the satellite imagery and the radar. The white portions of each echo represent areas of tornado threat. Tornadoes indicated by asterisks occurred at 2308 GMT beneath cluster 6, at 2315 GMT beneath complex 3, and at 2315 GMT beneath cluster 5. A new threat area in the storm at 9 is evident in both the radar and satellite imagery.

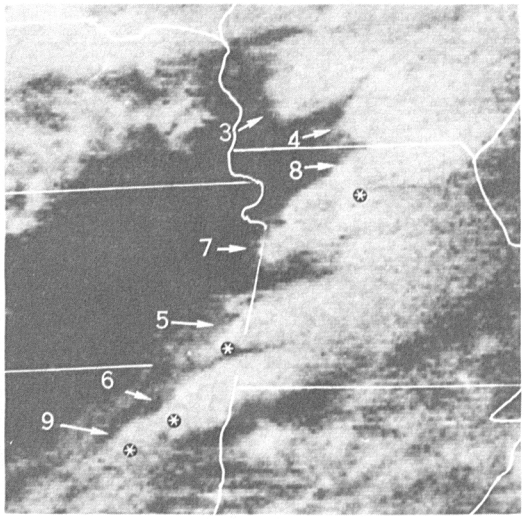

ATS-3 Frame 45 2347 GMT May 5, 1971 Radar Echoes 2347 GMT May 5, 1971

Figures 5-E-6m and n. A significant amount of detail is lost in the ATS picture because of poor solar illumination; however, most of the clusters are still easily detected. Tornadoes (*) were underway beneath clusters 5, 6, 8, and 9 at the time of this picture.

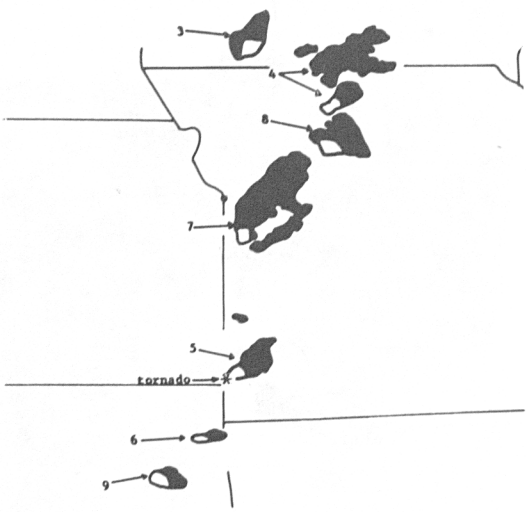

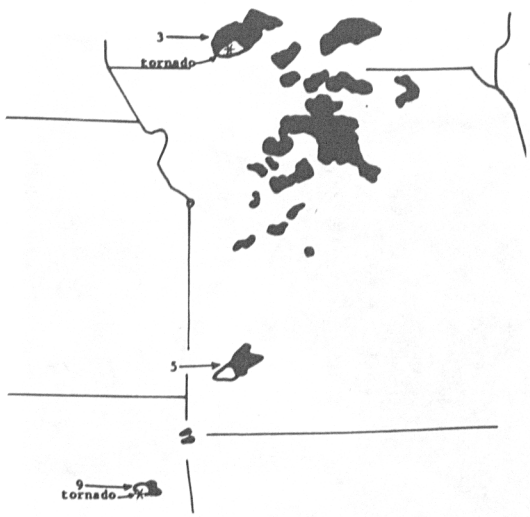

Radar Echoes 0007 GMT May 6, 1971 Radar Echoes 0045 GMT May 6, 1971

Figures 5-E-6o and p. Although no ATS imagery was available because of insufficient illumination for picture taking, the known threat areas were followed on radar. A devastating tornado (indicated by * in cluster 5) occurred in Joplin, Missouri at 0000 GMT, May 6, 1971. A tornado was reported beneath cluster 9 at 0044 GMT, and another beneath cluster 3 at 0045 GMT.

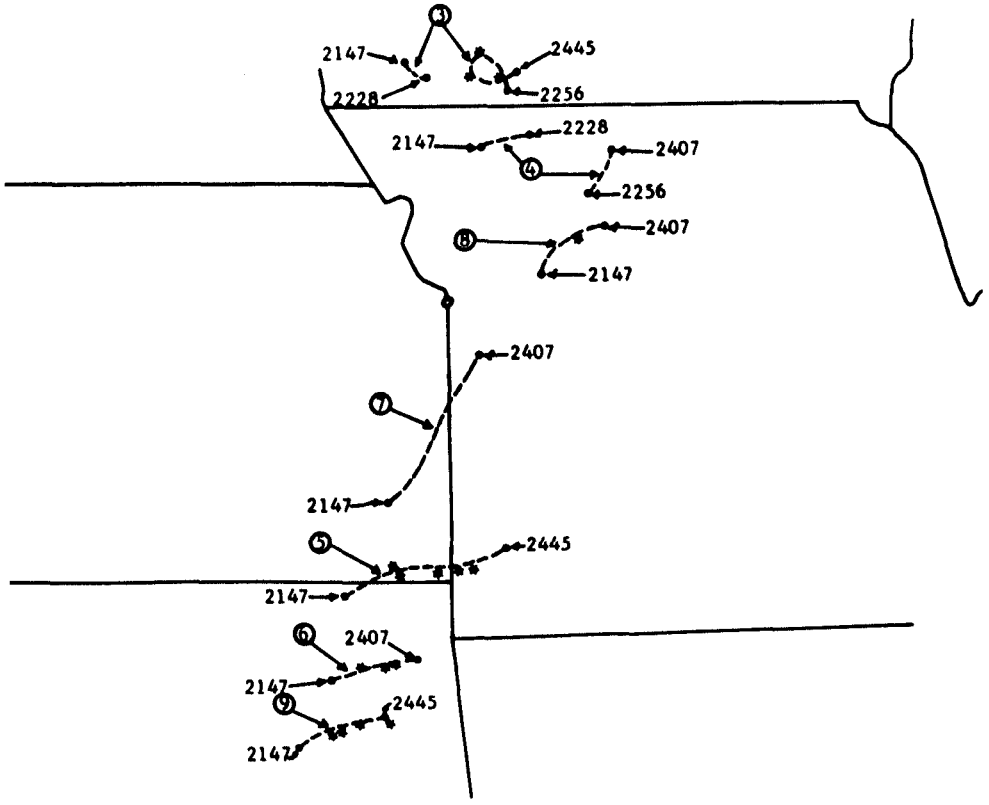

Threat Area Summary

Figure 5-E-6q. This figure shows the tracks of the center of each of the tornado threat areas (dashed lines) and the relationship of each track to the tornadoes which were reported. The GMT times that each threat area was first identified, plus the time it was last recognized, are also indicated. Each star (*) represents one tornado report; notice that no tornadoes occurred outside of a threat area. The threat tracks of the tornado-producing storms are all oriented at a far greater angle to the right of the low-level flow than those of the non-tornado producers. This indicates that the tornado-producing thunderstorms were all cyclonically rotating, right-deviating severe storms, while the slight right-offset of the non-tornado producers is due to the eastward progression of the squall line.

Chapter 5

Section F

Sea Breeze

Introduction

The existence of a sea breeze has been acknowledged by meteorologists for many years, but its region of influence was considerably underestimated until observations were made from satellites. Numerous investigations of the sea breeze show that many factors influence its development. At any particular location such things as the temperature difference between the land and sea surface, the strength and direction of the large-scale gradient-wind flow, the stability of the air mass which overlies the land and adjacent water, topography, friction, and the earth's rotation influence the sea breeze (71). Each coastal station must develop its own sea breeze study because the net effect of the parameters that influence the development of a sea breeze differs from station to station.

The basic cause of the sea breeze is the differential heating of adjacent land and water masses. Equal insolation over the land and adjacent water yields a higher air temperature over the land. The warmer air over land rises and is replaced by denser air. This denser air comes primarily from over the water because of the density gradient established by the differential heating. To compensate for the landward movement of the marine air, a portion of the air at a level above the ground drifts seaward and subsides, thus, creating a closed circulation cell (72). After its initial development, the sea breeze cell is located near the shoreline in the morning and then expands both landward and seaward as the day progresses. This expansion is not symmetric about the shoreline. The greatest expansion normally occurs over the water and may vary from approximately 10 to 20 miles out to 100 or more miles depending on the strength of the sea breeze cell. The inland penetration may vary from a few miles on steep, mountainous coastlines to 100 or more miles on flat, unobstructed coastlines. Vertically, the sea breeze may vary from as little as 50 feet up to as much as 8,000 feet, depending on the strength of the onshore flow (72). The maximum sea breeze flow is normally located between 100 and 200 feet above the surface.

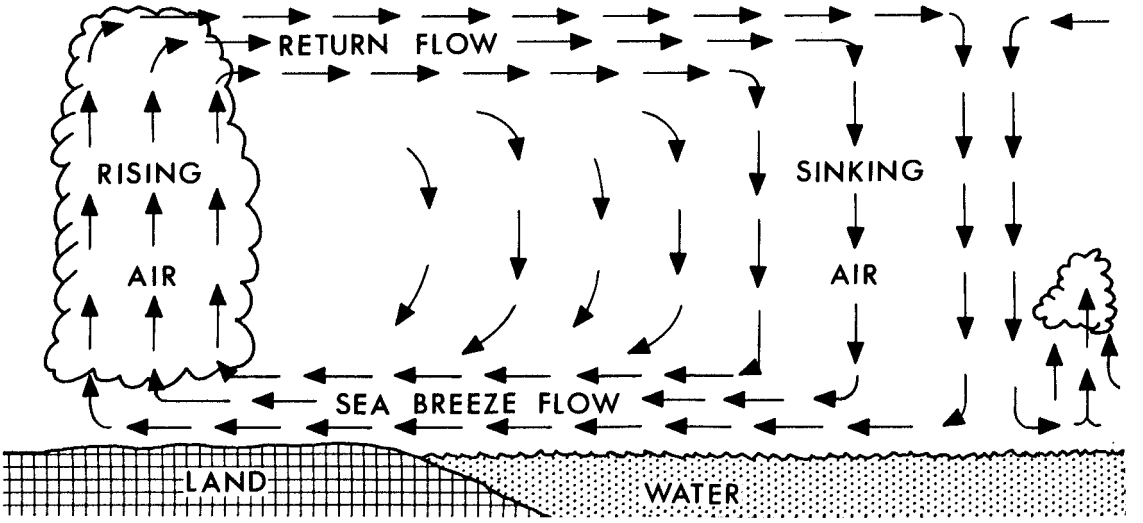

Figure 5-F-1. A schematic showing the classical sea breeze cell.

One of the most striking features of the sea breeze is the front-like zone at its leading edge over land. This zone, commonly referred to as the sea breeze front, moves inland as the sea breeze cell expands and then, as the cell deteriorates, moves seaward. The sea breeze front may result in showers as it moves inland, accompanied by a slight drop or leveling off of the temperature, a humidity change, and a wind direction change. As the sea breeze front moves seaward, its intensity will normally be decreasing, but may still result in showers, a humidity change, and a wind direction change.

In the case of a peninsula or an island, sea breeze circulations can develop along opposite shores. These multiple sea breeze zones lead to an area of increased convergence over the central region of the island or peninsula. The shape of a coastline also has an effect on the sea breeze. Various coastline curvatures result in convergence or divergence of the sea breeze flow.

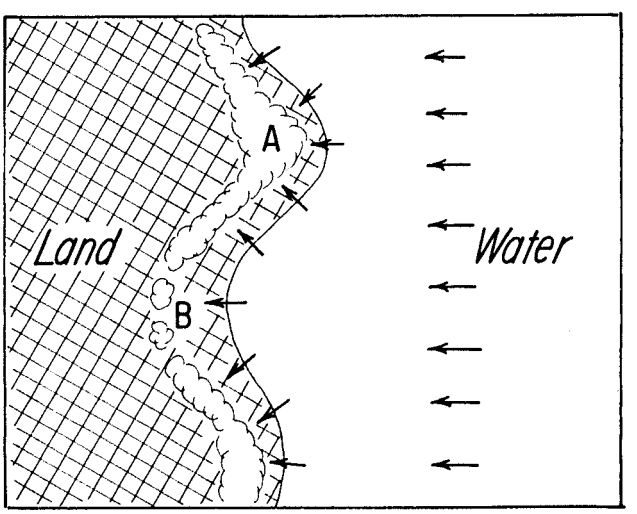

Figure 5-F-2. Schematic showing the relationship between coastline curvature and sea breeze frontal cloudiness.

Assuming a uniform, steady sea breeze flow onto an uneven coastline, the frictional drag acting on the flow over land results in mass convergence at A and mass divergence at B. These effects are portrayed by strengthening at A and weakening at B in the cloud pattern associated with the sea breeze front.

Sea Breeze Cloud Patterns

The effect of the sea breeze appears on satellite photographs as a line of clouds (sea breeze front) inland from the coast with a relatively cloud-free region along and off the coastline. The sea breeze front may or may not be continuous depending on terrain and other effects. The clear area ends abruptly over water where either random cloudiness or another line of clouds appears. The vertical development of this secondary line of clouds over the water in most cases is less than the vertical development of the line of clouds inland from the coast.

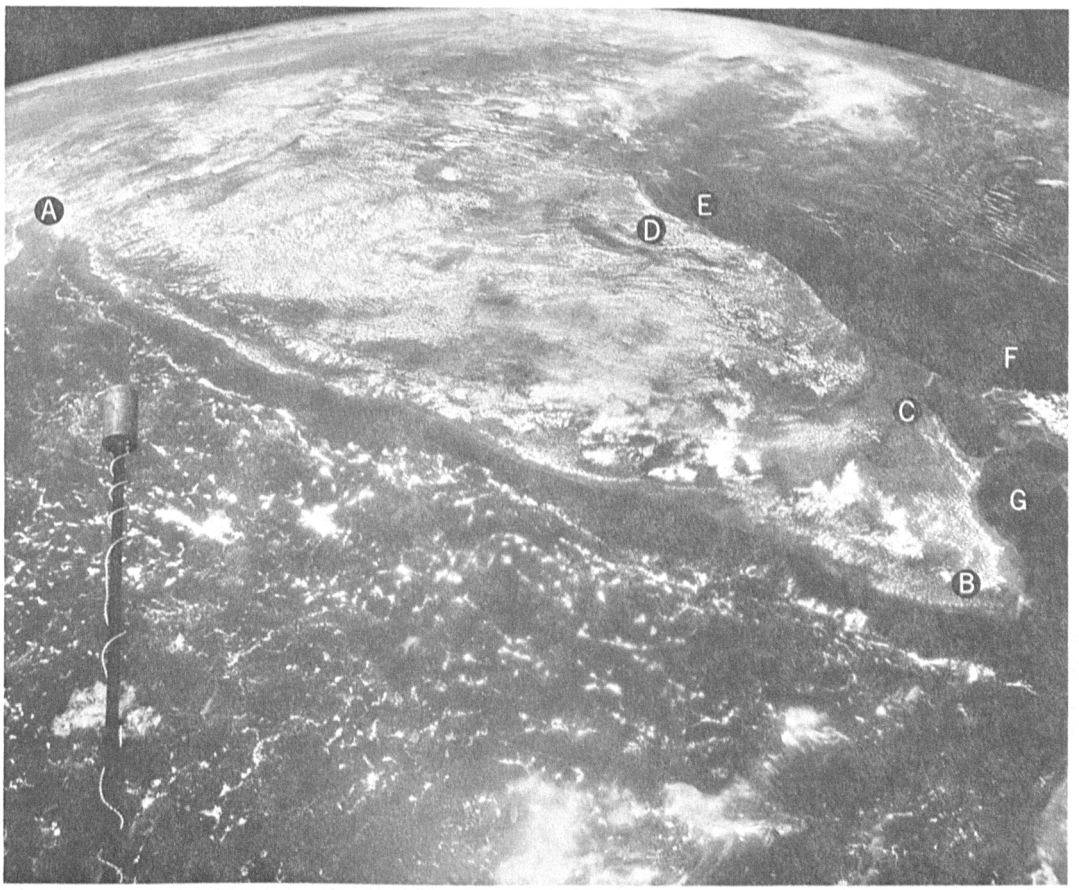

Gemini XI Orbit 26 Frame 27 September 14, 1966.

Figure 5-F-3. The cloud pattern resulting from a well-developed sea breeze is apparent along the entire western coast of India (A to B). The sea breeze front is seen inland from the coast. The cloud-free area associated with the sea breeze circulation extends seaward about 30 miles. Other sea breeze fronts exist along the southern and eastern coast of India from B to C to D. The extensive clear areas E, F, and G off the east coast are attributed to the sea breeze circulation cell and also to the effects of persistent upwelling (73).

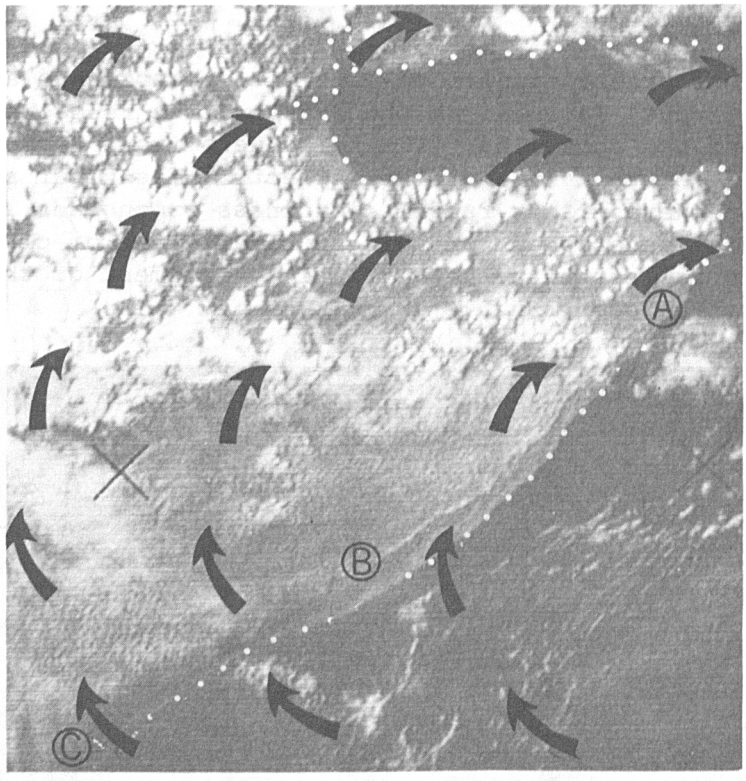

ITOS-1 3027-6 1029 GMT September 22, 1970.

Figure 5-F-4. This is an example of the cloud pattern resulting from a sea breeze which has developed along the coast of the Somali Republic. From A to B, the sea breeze front appears as a line of clouds about 30 miles inland. Offshore, the subsidence zone is clear. From B to C, the sea breeze circulation has produced onshore clearing, but no inland cloud line is present. This may be due to divergence in the low-level wind flow in this region. Arrows show the wind flow at the gradient level.

Observational studies of the sea breeze (74) show that when the gradient wind flow is directed onshore, thus reinforcing the sea breeze, the sea breeze front will penetrate further inland and will be more intense than with an offshore gradient wind flow. The clouds associated with a sea breeze front in most cases will have a greater horizontal and vertical extent with an onshore flow than with an offshore flow. The subsidence region associated with the sea breeze circulation will be well defined in both cases. Occasionally, with an onshore gradient flow, the advection of clouds into the subsidence region makes the seaward extent of the subsidence less apparent.

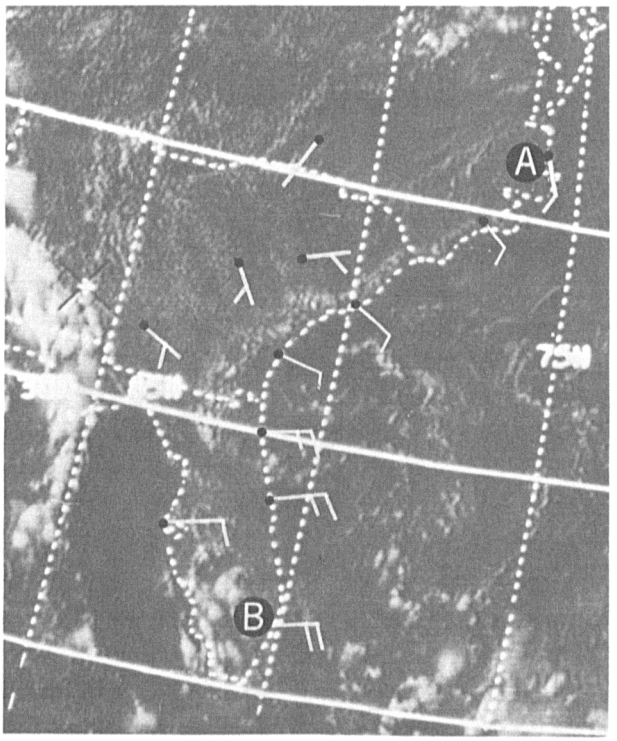

Figure 5-F-5. The cloud pattern resulting from a sea breeze is seen along the southeast coast of the United States from near Cape Hatteras (A) to just south of Miami (B). The sea breeze front has moved inland 50 or more miles over Georgia and Florida assisted by a strong easterly gradient-wind flow. The subsidence region off the coast is ill-defined in some areas, due to the advection of clouds into the area. Surface wind reports are shown on the picture.

ITOS-1 3044-4 1923 GMT September 23, 1970

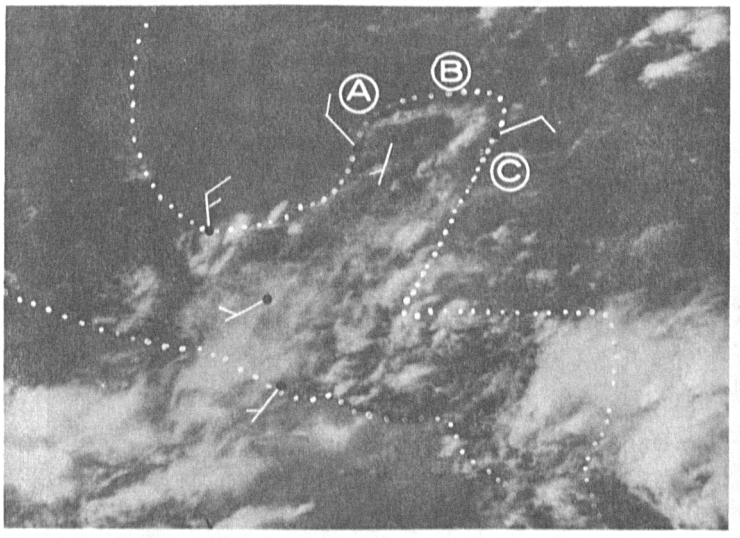

Figure 5-F-6. This is an example of the cloud pattern associated with the sea breeze along the north coast (A-B-C) of the Yucatan Peninsula. The inland penetration of the sea breeze front varies from approximately 10 miles on the northwest coast to 20 miles on the north and northeast coasts. The offshore subsidence regions are apparent at A and B, while at C, some clouds are being advected into the region by a northeast gradient-wind flow. The sea breeze front is enhanced by the onshore gradient-wind flow along the north and northeast coasts. Surface wind reports appear on the picture.

ATS-3 Frame 14 2004 GMT June 15, 1970

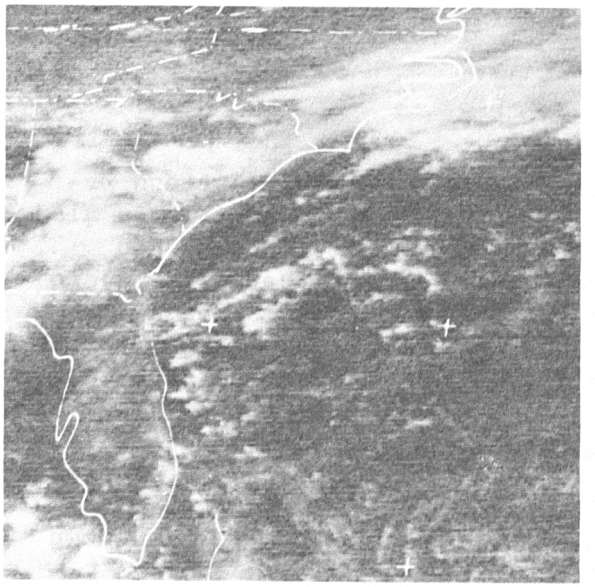

Figure 5-F-7a. ATS-3 Frame 2 1344 GMT August 28, 1970.

Figure 5-F-7b. ATS-3 Frame 5 1502 GMT August 28, 1970.

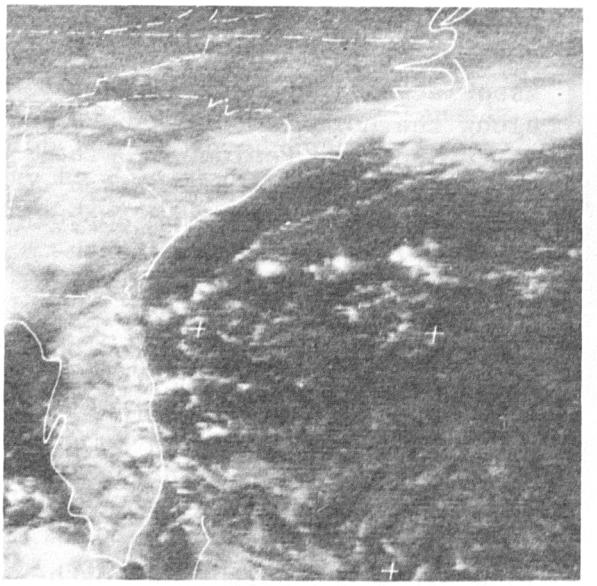

Figure 5-F-7c. ATS-3 Frame 7 1555 GMT August 28, 1970.

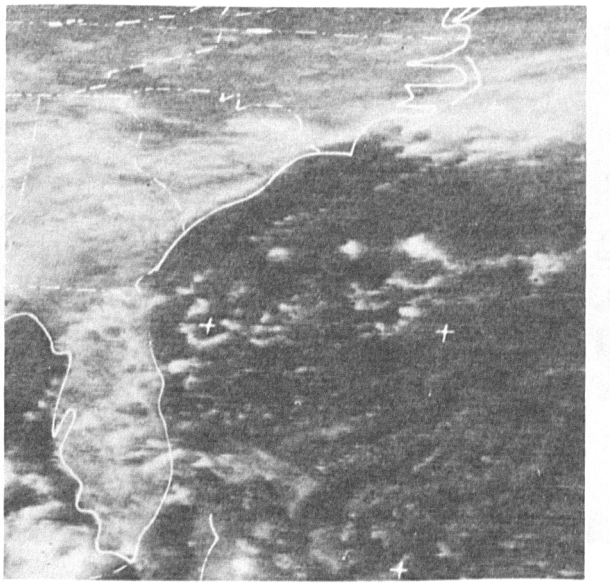

Figure 5-F-7d. ATS-3 Frame 10 1654 GMT August 28, 1970

Figure 5-F-7e. ATS-3 Frame 12
1747 GMT August 28, 1970.

Figure 5-F-7f. ATS-3 Frame 15
1905 GMT August 28, 1970.

Figures 5-F-7(a-f). This series portrays the development of the sea breeze along the southeast coast of the United States from North Carolina to southern Florida. The time period of the series is approximately 5½ hours. In photograph (a), the sea breeze is in its initial stage of development, with just a slight dissipation of the low clouds along the coast from North Carolina to northern Florida. In photograph (b), the sea breeze is stronger and more fully reflected in the cloud pattern. The low clouds along and off the coast from North Carolina to northern Florida dissipated as subsidence associated with the sea breeze cell increased. In photograph (c), the subsidence region expanded and became noticeable along the entire east coast of Florida. A faint line of clouds along the seaward edge of the subsidence region can also be seen from North Carolina to Florida. In photograph (d), the sea breeze front is just along the South Carolina and Georgia coasts, while over Florida it is developing further inland. The subsidence region continues off the coast. In photograph (e), the subsidence region continues to expand seaward and the clouds associated with the sea breeze front continue to develop. In photograph (f), the sea breeze front has pushed further inland along the entire coast and the clouds show significant vertical development. The subsidence area offshore remains quite large and easily recognized.

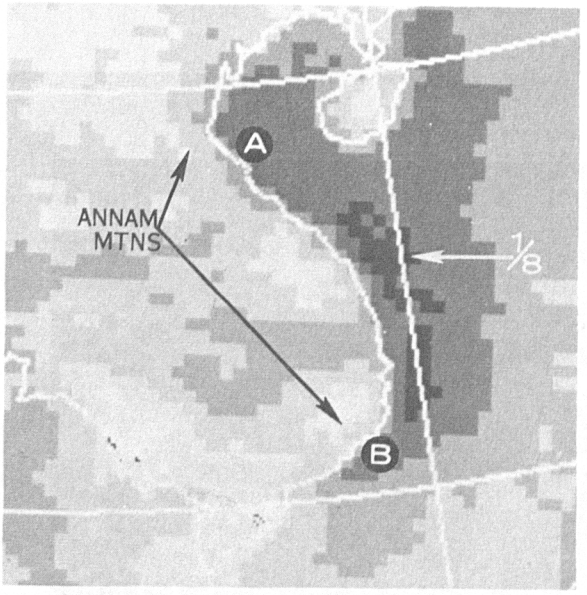

Figure 5-F-8a. Mean Eighths of Relative Cloud Cover for June.

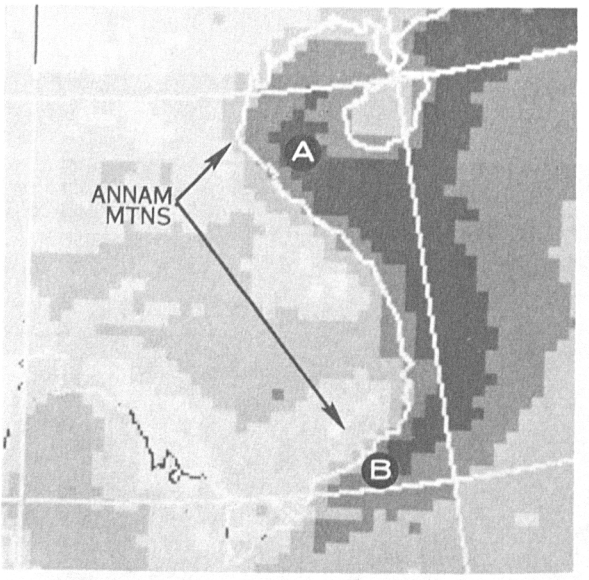

Figure 5-F-8b. Mean Eighths of Relative Cloud Cover for July.

Figure 5-F-8(a-c). These photographs are examples of satellite cloud climatology based on four years of satellite imagery near 1400 local time (75). Mean cloud cover in these pictures is depicted in nine gray shades. The darkest shade represents clear skies while the whitest shade represents overcast clouds. Each intermediate, brighter, gray shade corresponds to an increase of one-eighth mean cloud cover. The summer months shown are the period of the Southwest Monsoon over Southeast Asia.

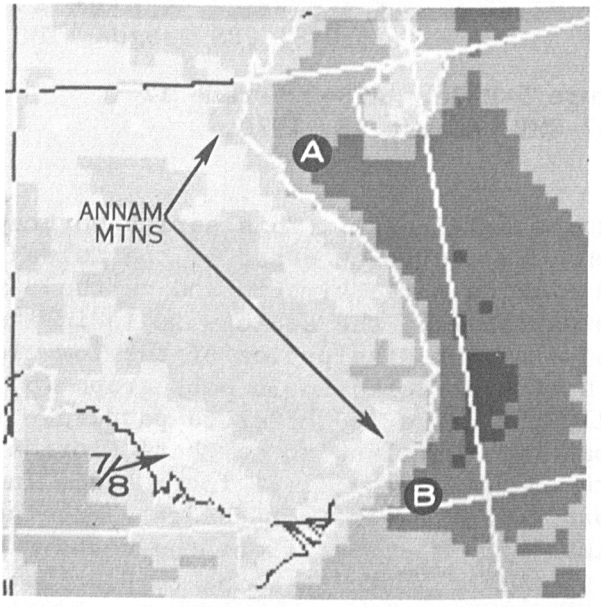

Figure 5-F-8c. Mean Eighths of Relative Cloud Cover for August.

The Annam Mountain Range blocks the southwest gradient-wind flow which results in a period of light winds in the low levels along the coast. During the period, the sea breeze circulation is dominant along the east coast of Vietnam. The influence of the sea breeze circulation, accompanied by downslope effects to the lee of the mountains, is reflected in the mean cloud cover from point A to B by a low percentage of cloud cover due to the two effects.

(57) Huschke, R. E., 1959: "Glossary of Meteorology", American Meteorological Society, p. 55.

(58) Smith, A. H., 1971: "A Cyclonically Curved Jet Stream", Picture of the Month, Monthly Weather Review, Vol. 97, No. 2, pp. 136-137.

(59) Fritz, S., 1965: "The Significance of Mountain Lee Waves as Seen from Satellite Pictures", Journal of Applied Meteorology, Vol. 4, pp. 31-37.

(60) Byers, H. R., 1959: General Meteorology, McGraw Hill, pp. 481.

(61) Kadlec, P. W., 1966: "Flight Observations of Atmospheric Turbulence", Federal Aviation Agency, Final Report, Contract No. FA 66 WA-1449, 52 pp.

(62) Kadlec, P. W., 1965: "Flight Data Analysis of the Relationship Between Atmospheric Temperature Change and Clear Air Turbulence", Weather Bureau, Final Report, Contract No. Cwb-10888, 45 pp.

(63) Sorenson, J. E., 1968: "Thermal Patterns and Clear Air Turbulence", United Airlines Meteorology Circular No. 62, 88 pp.

(64) Wiegman, E. J., 1965: "The Distribution of Clear Air Turbulence Reports and Cloud Patterns as Seen in Satellite Photographs", Stanford Research Institute, Final Report, Contract Cwb-10791, 101 pp.

(65) Foltz, H. P., 1967: "Prediction of Clear Air Turbulence", Colorado State University, Atmospheric Science Paper No. 106, 145 pp.

(66) Woolridge, G. and P. F. Lester, 1969: "Detailed Observations of Mountain Lee Waves and a Comparison with Theory", Colorado State University, Atmospheric Science Paper No. 138, 87 pp.

(67) Chopra, K. P. and L. F. Hubert, 1965: "Mesoscale Eddies in Wake of Islands", Journal of the Atmospheric Sciences, Vol. 22, No. 11, pp. 652-657.

(68) Miller, R. C., 1967: "Notes on Analysis and Severe-Storm Forecasting Procedures of the Military Weather Warning Center", Air Weather Service Technical Report #200, 91 pp.

(69) Frankhauser, J. C., 1971: "Thunderstorm-Environment Interactions Determined From Aircraft and Radar Observations", Monthly Weather Review, Vol. 99, No. 3, pp. 171-192.

(70) Newton, C. W., 1962: "Dynamics of Severe Convective Storms", National Severe Storms Project Report Number 9, U. S. Weather Bureau, Washington, D. C., 44 pp.

(71) Haurwitz, B., 1947: "Comments on the Sea Breeze Circulation", The Journal of Meteorology, Vol. 4, pp. 1-8.

(72) Schroeder, M. J., M. A. Fosberg, O. P. Cramer and C. A. O'Dell, 1967: "Marine Air Invasion of the Pacific Coast: A Problem Analysis", Bulletin of the American Meteorological Society, Vol. 48, No. 11, pp. 802-808.

(73) Raghavan, K., 1969: "Satellite Evidence of Sea Air Interaction During Indian Monsoon", Monthly Weather Review, Vol. 97, No. 12, pp. 905-908.

(74) Hsu, Shih-Ang, 1970: "Coastal Air Circulation System Observations and Empirical Model", Monthly Weather Review, Vol. 98, No. 7, pp. 487-509.

(75) Miller, D. B., 1971: "Four Years of Satellite Relative Daytime Cloud Cover over Southeast Asia", Proceedings, Chinese American Air Forces Technical Meteorological Workshop, Headquarters 1st Weather Wing, Hickam AFB, Hawaii.

U. S. GOVERNMENT PRINTING OFFICE : 1973 O - 499-830